

# The [OII] $\lambda$ 3727/H $\alpha$ Ratio of Emission Line Galaxies in the 2dF Galaxy Redshift Survey

M. Mouhcine<sup>1,2</sup>, I. Lewis<sup>3</sup>, B. Jones<sup>1,4</sup>, F. Lamareille<sup>5</sup>, S.J. Maddox<sup>1</sup>, T. Contini<sup>5</sup>

<sup>1</sup> School of Physics and Astronomy, University of Nottingham, Nottingham NG7 2RD

<sup>2</sup> Observatoire Astronomique de Strasbourg (UMR 7550), 11, rue de l'Université, 67000 Strasbourg, France

<sup>3</sup> Astrophysics, Nuclear and Astrophysics Laboratory, Keble Road, Oxford OX1 3RH

<sup>4</sup> Astronomy Unit, School of Mathematical Sciences, Queen Mary, University of London, Mile End Road, London, E1 4NS

<sup>5</sup> Laboratoire d'Astrophysique de Toulouse et Tarbes (LA2T - UMR 5572), Observatoire Midi-Pyrénées, 14 Avenue E. Belin, F-31400 Toulouse, France

Accepted ?. Received ?; in original form ?

## ABSTRACT

We investigate the systematic variation of the [OII] $\lambda$ 3727/H $\alpha$  flux line ratio as a function of various galaxy properties, i.e., luminosity, metallicity, reddening, and excitation state, for a sample of 1 124 emission-line galaxies, with a mean redshift  $z \sim 0.06$ , drawn from the Two Degree Field Galaxy Redshift Survey. The mean observed and extinction-corrected emission-line flux ratios agree well with the values derived from the *B*-band selected Nearby Field Galaxy Survey galaxy sample, but are significantly different from the values obtained from the H $\alpha$ -selected Universidad Complutense de Madrid Survey galaxy sample. This is because the different selection criteria applied in these surveys lead to a significant difference in the mean extinction and metallicity of different samples.

We use the  $R_{23}$  parameter to estimate the gas-phase oxygen abundance and find that the extinction-corrected [OII] $\lambda$ 3727/H $\alpha$  ratio depends on the oxygen abundance. For  $12 + \log(\text{O}/\text{H}) \gtrsim 8.4$ , we confirm that the emission-line ratio decreases with increasing metallicity. We have extended the relationship further to the metal-poor regime,  $12 + \log(\text{O}/\text{H}) \lesssim 8.4$ , and find that the correlation between the extinction-corrected [OII] $\lambda$ 3727/H $\alpha$  ratio and the metallicity reverses in comparison to the relationship for metal-rich galaxies. For metal-poor galaxies, in contrast with metal-rich ones, the variation of extinction-corrected [OII] $\lambda$ 3727/H $\alpha$  ratio is correlated with the ionization states of the interstellar gas.

The relative importance of the metallicity or the excitation state in determining the extinction-corrected [OII] $\lambda$ 3727/H $\alpha$  ratio depends on galaxy luminosity.

**Key words:** surveys, galaxies: fundamental parameters, galaxies: general, galaxies: statistics

## 1 INTRODUCTION

Spectral features in integrated spectra of galaxies allow us to determine important aspects of their evolutionary state. With the advent of the current generation of large telescopes, spectrophotometric studies are possible for fainter and more distant galaxies. Measuring the evolution of the star formation rate since the earliest cosmic epochs in the Universe is crucial for an accurate understanding of the formation and evolution of galaxies. Since the pioneering papers by Lilly et al. (1996) and Madau et al. (1996), several deep spectroscopic surveys have enabled detailed investigations of the star formation history of the universe (e.g., Hammer et al. 1997, Tresse et al. 2002, Hippelein et al. 2003).

The interpretation of integrated spectral properties, and estimates of the cosmic star formation rate over an extended redshift range requires the use of a range of star formation indicators. Unfortunately, there are significant discrepancies between different star formation rate indicators (Hopkins et al. 2003, and reference therein). The flux of the H $\alpha$  Balmer line is directly linked to the total ionizing flux, making this line the most robust and reliable tracer of star formation. H $\alpha$  emission line still suffers from attenuation by dust however. The [OII] $\lambda$ 3727 emission line has been used widely in a number of studies of the star formation rate in redshift ranges where the H $\alpha$  emission line moves into the near-infrared (e.g., Thompson & Djorgovski 1991; Cowie et al.

arXiv:astro-ph/0511809v1 29 Nov 2005

1997; Hogg et al. 1998; Hippelein et al. 2003). However, published calibrations of the star formation rate in terms of the [OII] $\lambda$ 3727 emission vary by factors of a few (Gallagher et al. 1989; Kennicutt 1992; Guzmán et al. 1997; Rosa-González et al. 2002).

Jansen et al. (2001) and Kewley et al. (2004) used the Nearby Field Galaxy Survey (Jansen et al. 2000, NFGS hereafter), and Aragón-Salamanca et al. (2005, submitted) the H $\alpha$  selected Universidad Complutense de Madrid Survey (UCM) to investigate the variation of [OII] $\lambda$ 3727 as a function of galaxy properties. Kewley et al. (2004) have found no systematic difference between star formation rates using H $\alpha$  and [OII] $\lambda$ 3727 luminosities after correcting for the effects of internal extinction and metallicity on [OII] $\lambda$ 3727 luminosity. Unfortunately, these are relatively small surveys and they sample rather limited ranges of interstellar gas parameters.

Since the pioneering works by Gallagher et al. (1989) and Kennicutt (1992), several spectroscopic studies of galaxies in the Local Universe have been undertaken (e.g., Tresse et al. 1999, Salzer et al. 2000, Jansen et al. 2000, Carter et al. 2001, Gavazzi et al. 2004). However, the number of emission line galaxies observed in these surveys for which *all* the emission lines needed to identify the nature of the ionizing source *and* to estimate gas phase metallicity (i.e., [OII] $\lambda$ 3727, H $\beta$ , [OIII] $\lambda$ 4959,  $\lambda$ 5007, [NII] $\lambda$ 6548, H $\alpha$ , [NII] $\lambda$ 6584, [SII] $\lambda$ 6717, and [SII] $\lambda$ 6731) are observed with high confidence do not exceed a few hundred galaxies at best. The advent of large spectroscopic surveys, such as the Sloan Digital Sky Survey (Stoughton et al. 2002, Abazajian et al. 2003, SDSS hereafter) and Two Degree Field Galaxy Redshift Survey (Colless et al. 2001, 2dFGRS hereafter) provides larger emission line galaxy samples with all the needed emission lines.

The 2dFGRS was carried out with the primary aim of studying the three-dimensional clustering properties of galaxies and determining the luminosity function. However for a subsample of the 2dFGRS galaxies, the quality of the spectra is good enough to determine accurate emission line properties. We select normal star forming emission line galaxies with strong emission lines, high-quality spectra, and high signal-to-noise for a detailed study of the sensitivity of [OII] $\lambda$ 3727/H $\alpha$  flux ratio to galaxy and interstellar medium properties. We aim to establish the properties of a local sample that can be used as a comparison for more distant galaxy samples. The 2dFGRS spectra are suitable for carrying out such an investigation, and have the following properties: (i) the large spectral coverage means that the galaxy spectra contain most of the prominent optical emission lines, including [OII] $\lambda$ 3727 and H $\alpha$ , and emission lines needed to identify the ionizing source, (ii) we can correct H $\alpha$  and H $\beta$  for the absorption features in the spectrum of the underlying stellar population.

The paper is organized as follows. In Sect.2, we describe how we obtain the emission line galaxy sample used in this paper from the original 2dFGRS data set. In Section 3, we describe surface photometry measurements of the 2dFGRS galaxies, and assess the effects of aperture on the emission line properties. Section 4 discusses the dependence of emission line [OII] $\lambda$ 3727/H $\alpha$  flux ratio on interstellar gas properties. In Sect. 5, we present the results of this analysis and summarize our conclusions.

Throughout this paper, all calculations assume the cos-

mology given by *WMAP*, with  $\Omega_{\Lambda} = 0.73$ ,  $\Omega_m = 0.27$  and  $H_0 = 71 \text{ km s}^{-1} \text{ Mpc}^{-1}$  (Spergel et al. 2003).

## 2 GALAXY SAMPLE

Our sample is drawn from the 2dFGRS data set, which consists of optical (3600-8000 Å) spectroscopy of more than 250 000 galaxies brighter than  $b_j = 19.7$ , with a full width at half-maximum (FWHM hereafter) spectral resolution of 9 Å. The survey covers two contiguous declination strips, plus 99 randomly located fields. One of the strips is located close to the south Galactic pole, while the other strip is located on the celestial equator in the northern Galactic hemisphere. Full details of the survey strategy are given in Colless et al. (2001).

We first exclude all galaxies observed before 31 August 1999, since these were observed whilst there was a fault with the atmospheric dispersion compensator within the 2dF instrument (Lewis et al. 2002a). For these galaxies, the fitting procedure to determine the line properties gives results of poor quality. This cut leaves us with 200 160 galaxies. We selected galaxies with high quality redshift determinations, reducing the sample to 185 731 galaxies. We used a fully automatic procedure to measure the emission lines properties. A detailed discussion of the procedure and the determination of the fitting quality is presented by Lewis et al. (2002b). Here we summarize the basic points of this procedure. The line fitting consists of a simultaneous fitting of a series of absorption lines and a series of emission lines. Some of these are very close in wavelength (e.g., H $\beta$  in absorption and emission). This technique works very well in fitting broad absorption lines and narrow emission lines (see figure 2 in Lewis et al. 2002b). The fitting allows a common wavelength shift for all the lines so relative shifting between the lines is not allowed. It does not work as well for broad emission lines where the absorption component is not well constrained or where several emission lines can combine to give a non-unique solution (e.g., [NII] $\lambda$ 6548 and H $\alpha$ ). These results are however, good enough to identify broad emission line cases. Note that only high signal-to-noise (S/N) spectra have been fitted. To get accurate estimates of the gas phase properties, and to avoid any possible bias, we select galaxies having a good quality fit for *all* of the emission lines needed to classify the galaxies, i.e., the nature of the ionizing sources, and to measure the gas-phase oxygen abundance. This requirement leaves us with a sample of 10 284 galaxies. Equivalent widths were corrected from the observed to the rest frame. We select only galaxies whose spectra have a relatively high S/N ratio, i.e.  $S/N \geq 10$  measured on the continuum between 4000 Å and 7500 Å. This leaves us with a sample of 7 353 galaxies. In our subsequent analyses, we use only galaxies which show Balmer lines in emission with equivalent widths larger than 10 Å after correcting for the underlying stellar absorption. This corresponds to the spectral resolution of the 2dF instrument, and galaxies with weaker emission are subject to large systematic uncertainties from instrumental effects, particularly affecting estimates of the internal dust extinction from the Balmer decrement. This equivalent width threshold also minimizes the effect of the underlying stellar absorption. The requirement of having the H $\beta$  equivalent width larger than the spectral resolution of the 2dF

instrument drastically reduces the number of emission line galaxies in the final sample, and leaves us with 1327 galaxies.

As we are interested in normal emission line galaxies, we have excluded galaxies which are dominated by Active Galactic Nuclei (AGN hereafter). We first exclude galaxies which have a  $\text{H}\beta$  emission line FWHM larger than  $10 \text{ \AA}$  (corresponding to a velocity width of  $\gtrsim 670 \text{ km s}^{-1}$ ), since these are likely to be Seyfert I galaxies. We then use the classical diagnostic ratios of two pairs of relatively strong emission lines (Baldwin et al. 1981, Veilleux & Osterbrock 1987) to distinguish between galaxies dominated by emission from star-forming regions and galaxies dominated by emission from non-thermal ionizing sources. We classify galaxies according to their position in  $[\text{OIII}]\lambda 5007/\text{H}\beta$  vs.  $[\text{NII}]\lambda 6583/\text{H}\alpha$  and  $[\text{OIII}]\lambda 5007/\text{H}\beta$  vs.  $[\text{SII}]\lambda 6717, \lambda 6731/\text{H}\alpha$  diagrams. The demarcation between star-forming galaxies and AGN in both diagrams was taken from Kewley et al. (2001). Fig. 1 shows the distribution of the sample galaxies in the diagnostic diagrams. We used the conservative requirement that a galaxy must be classified as a star-forming galaxy in both diagnostic diagrams in order to be retained in our sample (see Lamareille et al. 2004 for more detail on the classification of emission line objects). The diagrams show that our sample contains galaxies with a large range of excitation levels, suggesting that our sample contains both metal-rich and metal-poor galaxies. This sample is thus suitable for studying the properties of dust obscuration and emission lines over a large range of metallicities and excitation parameters.

196 galaxies show Balmer decrements smaller than the intrinsic  $\text{H}\alpha/\text{H}\beta$  ratio of 2.85 which corresponds to case B recombination with a temperature of  $T = 10^4 \text{ K}$ , and a density of  $n_e \sim 10^2 - 10^4 \text{ cm}^{-2}$  (Osterbrock 1989). This is probably due to an intrinsically low extinction, coupled with uncertainties in the correction of the underlying stellar absorption, and/or errors in the data reduction. As this implies a physically impossible negative extinction, those galaxies were removed from the sample. Thus, we end up with a final sample of 1124 normal emission line galaxies.

The distributions of global properties, i.e., galaxy colours,  $b_j$ -band absolute magnitudes, redshift, and the  $\eta$  parameter respectively, of the selected sample are shown in Fig. 2. The corresponding numerical data for emission line galaxy properties presented in this paper are provided for the reader through CDS\*, or directly from the authors. The parameter  $\eta$  is a linear combination of the first two projections derived from the Principal Component Analysis of the 2dFGRS spectra. This parameter is found to be a measure of galaxy spectral type, i.e., a measure of the average emission/absorption line strength of a galaxy (see Madgwick et al. 2002 for a detailed discussion). As one may expect, the final emission line galaxy sample contains galaxies with bluer colours and later spectral types than the bulk of galaxies in the parent 2dFGRS sample. As a result of the selection procedure, the redshifts in the final emission line galaxy sample do not exceed  $z \sim 0.13$ , with a median around  $z \sim 0.06$ . The observed gaps in the redshift distribution occur when one or

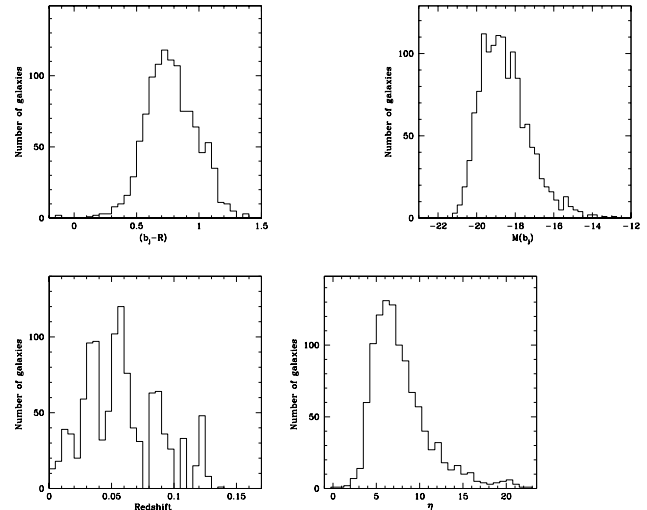


**Figure 2.** Distribution of general properties of our sample of 1124 star forming galaxies. The upper panels show the absolute  $b_j$ -band magnitude, and  $(b_j-R)$  colour distributions. The lower panels show the distributions of redshift and the spectral type-sensitive parameter  $\eta$ .

more of the emission lines lie close to a night-sky emission line, reducing the signal-to-noise ratio around that line, and hence the quality of the line fitting, which cause them to be excluded them from the final emission line galaxy sample.

The completeness of the final galaxy sample is difficult to quantify, and it is possible that the selection procedure could disguise the existence of intrinsic correlations between galaxy properties that we aim to investigate. Therefore it is important to assess to what extent the final sample of emission line galaxies covers similar regions in the parameter space (e.g., luminosity, colour, spectral type, surface photometry properties) as emission line galaxies in the original 2dFGRS sample. To ensure that our final sample of emission line galaxies is representative of the parent 2dFGRS emission line galaxies, we compare the distribution of galaxy properties for both samples.

The parent 2dFGRS emission line galaxy sample was selected as follows. It contains objects in the final 2dFGRS data release having reliable redshifts, for which we have a reliable match between the APM target coordinates with the SuperCOSMOS Sky Survey image catalogue (Hambly et al. 2001). There is also the additional criterion that heliocentric radial velocities  $cz > 1000 \text{ km/s}$ . This constraint was added to guard against including any incorrect velocities caused by having a Galactic star superimposed on a galaxy image, or an outright failure of the redshift estimation. It also removes very nearby galaxies for which the velocity is a poor indicator of distance, and hence guards against getting incorrect absolute magnitudes: only a very small number of dwarf galaxies with  $M(b_j) > -15 \text{ mag}$  are rejected (a small number because the volume is small, and dwarfs because of the apparent magnitude limits of the survey). We have estimated the surface photometry parameters for 2dFGRS galaxies using blue images obtained from the SuperCOSMOS Sky Survey (see Sect. 3.1 for a detailed discussion of surface photometry measurements). The effective radius is

\* Centre de Données Astrophysiques de Strasbourg, <http://cdsarc.u-strasbg.fr/CDS.html>

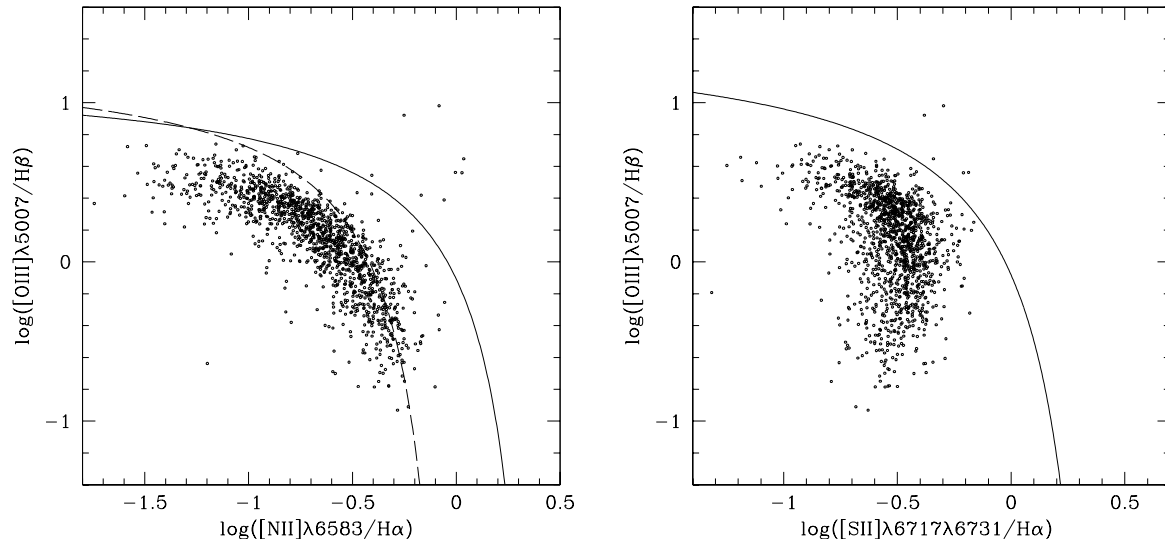


**Figure 1.** Diagnostic diagrams for our sample of 1327 narrow emission line galaxies. The continuous lines show the theoretical separation between starburst galaxies and AGNs from Kewley et al. (2001). The dashed line in the  $[\text{NII}]\lambda 6583/\text{H}\alpha$  vs.  $[\text{OIII}]\lambda 5007/\text{H}\beta$  diagram shows the separation between starburst galaxies and AGNs as defined empirically by Kauffmann et al. (2003) using SDSS data.

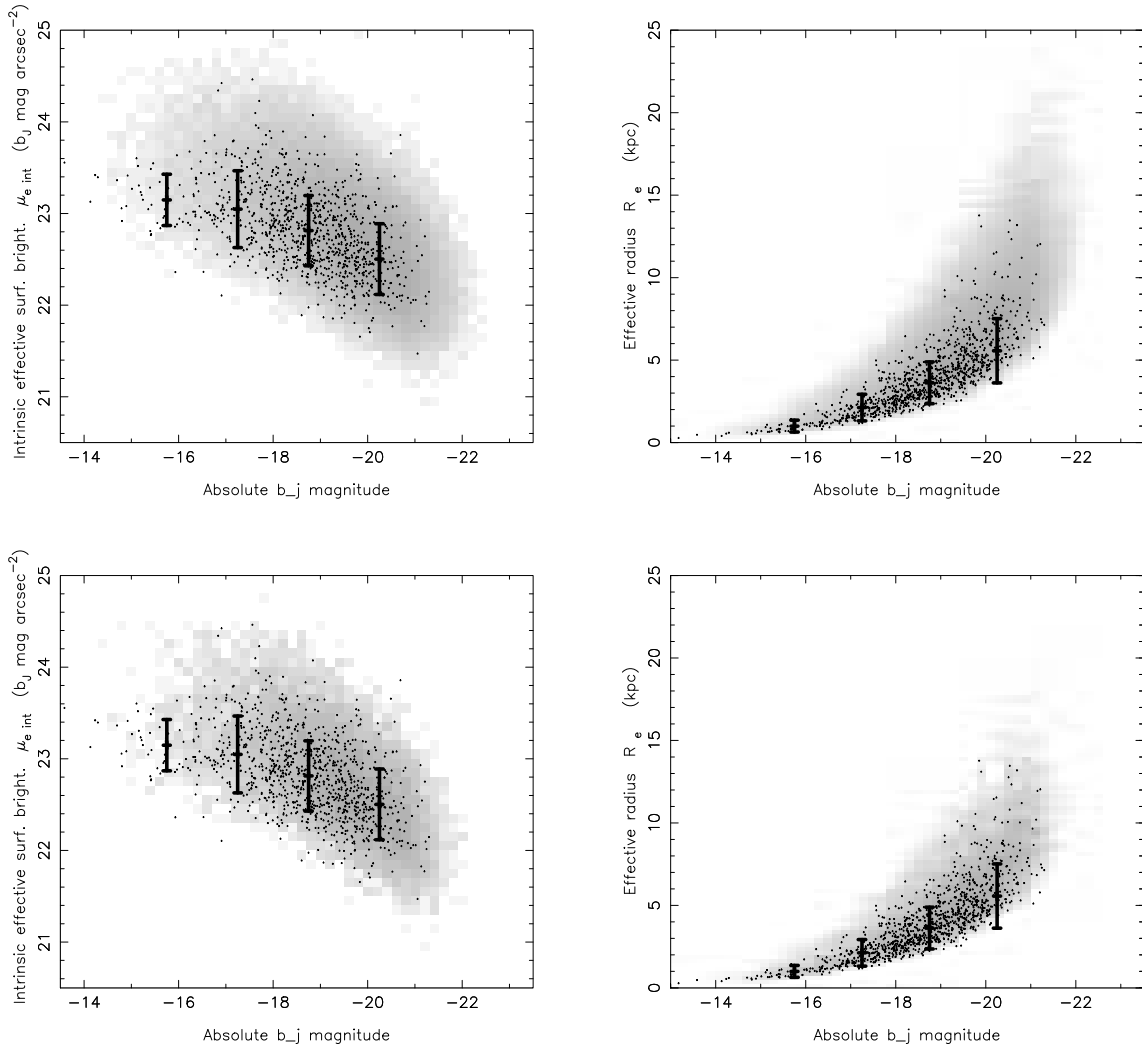
estimated as the semi-major axis of the ellipse that contains half the light of the galaxy, while the effective surface brightness is the surface brightness at the half-light isophote.

Fig. 3 shows the variation of intrinsic surface brightness and physical effective radius as a function of absolute  $b_j$ -band magnitude respectively (see Section 3.1 for details of the calculation of these quantities). Our 1124 galaxy sample is shown as dots, with the bars showing the medians and the standard deviations in 1.5 magnitude wide bins. The parent 2dFGRS emission line galaxy sample is shown as a greyscale plot on a logarithmic scale. For our sample galaxies, for which  $\text{H}\alpha$  equivalent widths are larger than  $\sim 25 \text{ \AA}$ , strong correlations are apparent between surface photometry properties and absolute magnitude, i.e., luminous/faint galaxies tend to have on average large/small physical sizes and high/low central surface brightness. The first parent 2dFGRS emission line galaxy sample, shown in the upper panels, was constructed from the 2dFGRS sample by selecting galaxies with  $\eta > 0$ , i.e.,  $\text{H}\alpha$  line in emission, and contains 71 207 galaxies. The comparison between the parent 2dFGRS emission line galaxy sample, and the final 1124 emission line galaxy sample shows that (i) the parent emission line galaxy sample includes luminous galaxies, i.e., brighter than  $M(b_j) \sim -21$ , that are excluded from the final 1124 emission line galaxy sample, and (ii) for a given galaxy magnitude, galaxies with low surface brightness and larger effective radii tend to be excluded from our final 1124 emission line galaxy sample. This is because galaxies in the final sample were selected on the basis of their  $\text{H}\beta$  equivalent width being larger than  $10 \text{ \AA}$ . To take this selection criterion into account, we have constructed a second parent 2dFGRS emission line galaxy sample by selecting galaxies from the 2dFGRS sample requiring both  $\eta > 0$  and  $\text{H}\beta$  equivalent width larger than  $10 \text{ \AA}$ . This second sample contains 12 660 galaxies. The bottom panels of Fig. 3 show a comparison between our 1124 emission line galaxy sample and the sec-

ond 2dFGRS parent emission line galaxy sample. It shows that emission line galaxies in the final emission line galaxy sample cover roughly similar ranges of galaxy parameters as the second parent 2dFGRS emission line galaxy sample, and that galaxies are distributed similarly in both samples. The cut on  $\text{H}\beta$  equivalent width excludes bright/physically big galaxies, since galaxies with low emission line equivalent width tend to dominate the bright end of the galaxy luminosity function (e.g., Salzer et al. 1989; Kong et al. 2002). Despite this cut, the final 1124 emission line sample covers a large range of galaxy luminosities, i.e., 7 magnitudes, similar to the magnitude range covered by NFGS sample (Jansen et al. 2000) or 15R-North galaxy redshift survey sample (Carter et al. 2001). This is attributed to the large scatter that affects the galaxy luminosity versus emission line equivalent width relation (e.g., Jansen et al. 2000). The distributions of the final 1124 emission line galaxy sample and the second parent 2dFGRS emission line galaxy sample are similar in both  $(b_j\text{-R})$  vs.  $\mu(b_j)$  and  $(b_j\text{-R})$  vs.  $R_e$  diagrams.

Fig. 4 shows the variation of  $(b_j\text{-R})$  colour,  $\text{H}\alpha$  equivalent width, and extinction-uncorrected  $[\text{OII}]\lambda 3727/\text{H}\alpha$  flux ratio (see below for a detailed discussion of the procedure we use to estimate this ratio) as a function of  $b_j$ -band magnitude for the final 1124 galaxy sample and the parent 2dFGRS emission line galaxy sample. Galaxies in the parent 2dFGRS sample were selected by having  $\eta > 0$  and  $\text{H}\beta$  equivalent width larger than  $10 \text{ \AA}$ . Again, the final 1124 galaxy sample is distributed similarly to the 2dFGRS parent sample of emission line galaxies with  $\text{H}\beta$  equivalent width larger than  $10 \text{ \AA}$ . The parent sample of emission line galaxies with  $\text{H}\beta$  equivalent width larger than  $10 \text{ \AA}$  contains galaxies with low  $\text{H}\alpha$  equivalent width, and high observed  $[\text{OII}]\lambda 3727/\text{H}\alpha$  flux ratio that are not present in the final 1124 emission line galaxy sample. However, these galaxies represent less than 1% of the parent sample. The simi-





**Figure 3.** Comparisons between the properties of the final 1 124 emission line galaxy sample discussed in the remainder of the paper and those of the parent emission line samples. The 2dFGRS emission line galaxy sample is shown as a greyscale plot on a logarithmic scale, and the final galaxy sample is shown as dots. For top panels, galaxies in the parent emission line galaxy sample were selected from the 2dFGRS sample requiring  $\eta > 0$ . Top left: intrinsic effective surface brightness plotted against absolute  $b_j$ -band magnitude. Top right: physical effective radius against absolute  $b_j$ -band magnitude. For the bottom panel, galaxies in the parent emission line galaxy sample were selected are those with  $\eta > 0$  and  $\text{H}\beta$  equivalent width larger than  $10 \text{ \AA}$ . Bottom left: similar to the upper left panel. Bottom right: similar to the upper right panel. The final 1 124 galaxy sample covers similar ranges of galaxy parameters than the parent sample of 2dFGRS emission line galaxies with  $\text{H}\beta$  equivalent width larger than  $10 \text{ \AA}$ .

lar distributions of both emission line galaxy samples suggest that our final 1 124 galaxy sample is representative of the parent sample of 2dFGRS emission line galaxies with  $\text{H}\beta$  equivalent width larger than  $10 \text{ \AA}$  in terms of its luminosity, colour, and surface photometry properties. Also, the 2dFGRS spectroscopic sample is representative of the complete 2dFGRS magnitude-limited photometric sample down to the surface brightness limit of the 2dFGRS, i.e.,  $\sim 24.5 b_j \text{ mag arcsec}^{-2}$  (Cross et al. 2001). Hence, the final 1 124 emission line galaxy sample is fairly representative of the vigorously star forming, i.e.,  $\text{H}\beta$  equivalent width larger than  $10 \text{ \AA}$ , local emission line galaxies, within the 2dFGRS limits. The correlations we aim to investigate are expected then not to be severely biased by the selection procedure of the final sample of 1 124 emission line galaxies. However,

we can not rule out the possibility that we are missing faint galaxies with strong emission lines, but with low surface brightness, i.e., close to or lower than the 2dFGRS surface brightness limit.

### 3 APERTURE EFFECTS

The fibres in the 2dF instrument cover a 2.1 arcsecond diameter region of each galaxy, and this small aperture coverage of galaxies may bias the distribution of galaxy properties, and the estimate of the emission line properties (e.g., Kochanek et al. 2001). The aperture in fibre-fed spectroscopy is usually centred on the inner part of the galaxies so that the nuclear light is collected. For 2dFGRS, the in-

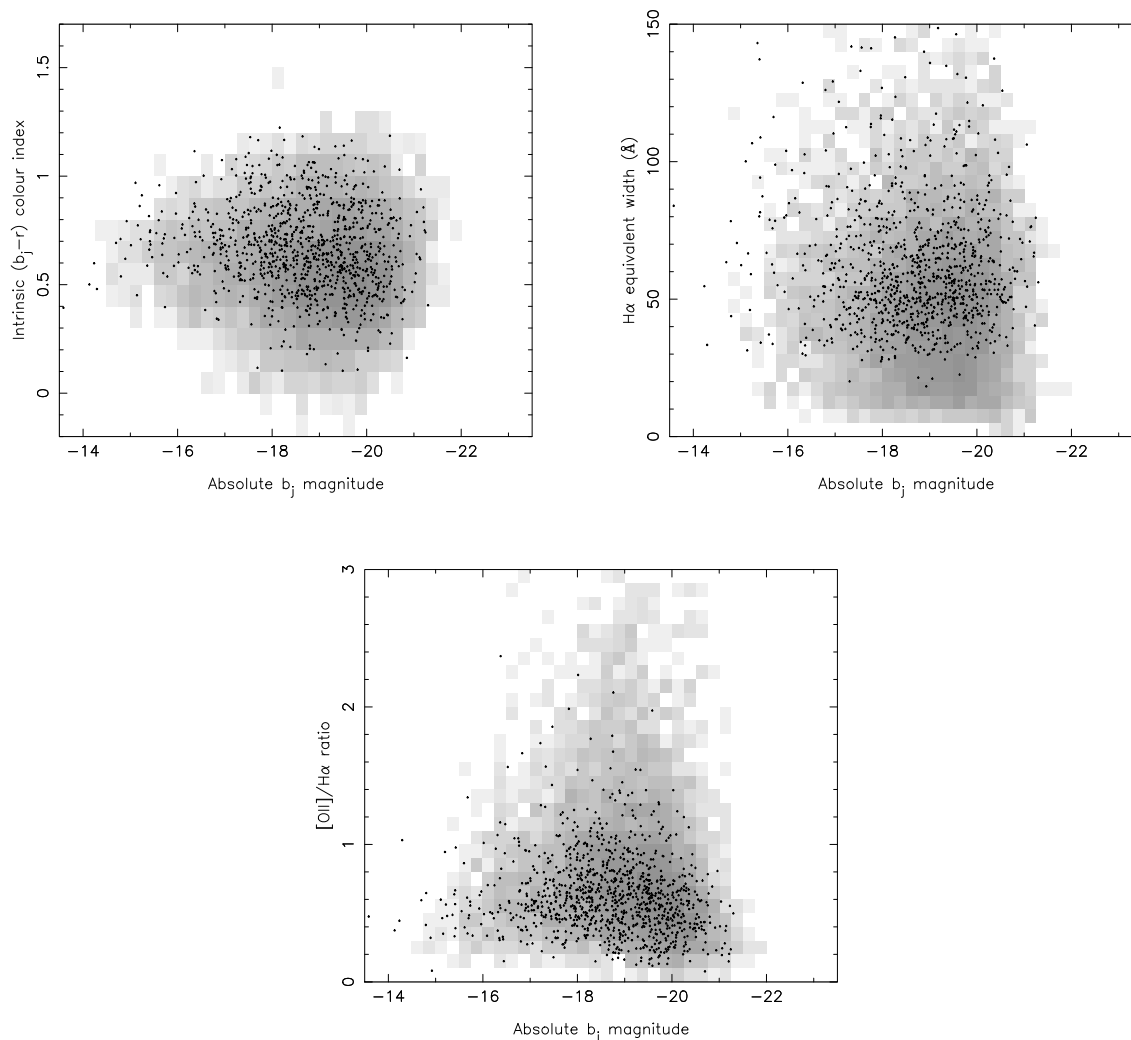


**Figure 4.** Comparisons between the variation of  $(b_j-R)$  colour (*left*),  $H\alpha$  equivalent width (*middle*), and observed  $[OII]\lambda 3727/H\alpha$  flux ratio (*right*), as a function of  $b_j$  magnitude for the final 1 124 emission line galaxy, shown as dots, and the parent emission line sample, shown as a greyscale plot on a logarithmic scale. The galaxies in the parent 2dFGRS emission line galaxy sample were selected as those with  $\eta > 0$ , and  $H\beta$  equivalent width larger than  $10 \text{ \AA}$ .

ternal precision with which the fibres are aligned with the galaxy centre is  $0.16 \text{ arcsec}$  on average, with no fibres outside  $0.3 \text{ arcsec}$  (Colless et al. 2001). The absolute accuracy of the input astrometry is  $\sim 0.5 \text{ arcsec}$  (Maddox et al. 1990a). The fraction of the light from outer parts of a galaxy will depend on its redshift, intrinsic size, and surface brightness profile, as well as the size of the fibre and seeing during the observation. The bias introduced by such observational procedure depends also on the morphological type of the observed galaxies. The larger the bulge-to-disk ratio, the more serious may be the potential bias. Even though the distribution of star-forming regions tend to be centrally distributed in bulge-dominated galaxies, luminous star forming regions tend to be located in the outer regions of the disk. The major caveat might come from irregular galaxies where star forming regions can be found anywhere. Aperture effects are therefore a concern, and we must assess how close the spectra of our sample galaxies are to fully integrated galaxy

spectra. We first consider the surface brightness profiles of the galaxies, to estimate the fraction of a galaxy’s light that is sampled by the fibre. We then search for any correlation between emission line properties and the fraction of light sampled.

### 3.1 Surface photometry of 2dFGRS galaxies

Surface photometry was carried out using blue image data from the United Kingdom Schmidt Telescope obtained from the SuperCOSMOS Sky Survey (Hambly et al. 2001, Hambly, Irwin & McGillivray 2001). Data were downloaded from the public Survey server in Edinburgh<sup>†</sup> for a  $2.0 \text{ arcmin}$  square region around each galaxy.

The SExtractor program (Bertin 1998, Bertin &

<sup>†</sup> <http://www-wfau.roe.ac.uk/sss/>

Arnouts 1996) was run over each data file and the SExtractor object corresponding to the 2dF target was identified, on the basis of a close match to the celestial coordinates of the 2dFGRS target. For each 2dF target, SExtractor provided the object centroid coordinates, an overall image ellipticity and the orientation of the object. This analysis used only those pixels having a surface brightness brighter than  $25.0 b_j \text{ mag arcsec}^{-2}$ . A series of concentric elliptical annuli were then defined on a linear scale for each 2dFGRS target which were centred on the image centroid of the target and had the overall image ellipticity and orientation. The mean SuperCOSMOS intensity was then measured within each annulus. The results from these annuli provided a surface brightness profile in the form of the mean intensity as a function of the semi-major axis of the annuli.

Exponential surface brightness profiles were fitted to the surface brightness profiles weighting each data point according to an estimate of the error in the intensity. These fits were performed between intensities corresponding to  $22.3$  and  $27.0 b_j \text{ mag arcsec}^{-2}$ . The bright limit was imposed to avoid problems associated with photographic saturation in the UKST survey data (e.g Maddox et al. 1990ab, Shao et al. 2003). Data points within  $1.5 \text{ arcsec}$  of the image centre were excluded to avoid any problems caused by the presence of a nucleus or by seeing. The fitted profile is characterised by the central surface brightness and the exponential scale length along the major axis. As the method avoids the saturated higher surface brightness regions of galaxy images, in the case of spiral galaxies it is mostly sensitive to their discs. The central surface brightness is therefore an extrapolation to the image centre of the fitted profile.

The SuperCOSMOS intensities were converted to magnitude surface brightnesses using calibrations for each UKST plate derived from the public SuperCOSMOS Sky Survey total magnitudes. The photometric zero point of the SuperCOSMOS data for each UKST plate was selected to minimise the differences between the total magnitude under the fitted exponential profile and the SuperCOSMOS Sky Survey total  $b_j$  magnitudes for all 2dFGRS targets within that UKST field. No attempt was made to account for photometric variations across individual UKST plates: the SuperCOSMOS Sky Survey pixel data have already been corrected for vignetting effects, and no strong evidence of residual effects were found during a comparison of the fitted profile data with total magnitudes from the APM Catalogue (Maddox et al. 1990a). The magnitude surface brightnesses of the fitted exponential profiles have therefore been put on to the SuperCOSMOS Sky Survey scale. The root-mean-square difference between the total magnitude under the fitted exponential profiles and the total magnitudes from the SuperCOSMOS Sky Survey Catalogue is  $0.15 \text{ mag}$ , which will be caused by factors including a failure to account for bulges of spiral galaxies, the  $r^{1/4}$  profiles of ellipticals and peculiar galaxy morphologies. This figure is slightly larger for lower redshifts and for lower surface brightnesses, but does not vary with colour. The data of Hambly, Irwin & MacGillivray (2001) indicate that the absolute calibration of the SuperCOSMOS Sky Survey Catalogue blue magnitudes is accurate at the  $0.1\text{--}0.2 \text{ mag}$  level.

The surface photometry gave the inferred central surface brightness  $\mu_{o, \text{obs}}$  and the angular scale length. To cor-

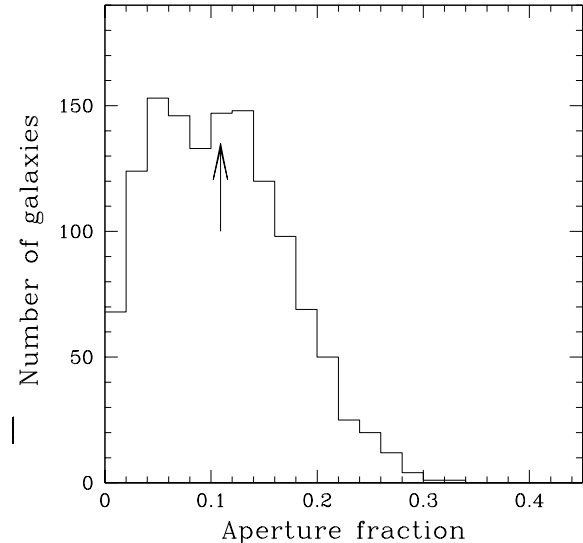


**Figure 5.** Distribution of the fraction of the total galaxy light observed by the fibre for the galaxy sample discussed in the paper. The vertical arrow indicates the location of the mean of the covering fraction distribution, i.e., 11%.

rect for cosmological surface brightness dimming, the intrinsic central surface brightness was computed as:

$$\mu_{o, \text{int}} = \mu_{o, \text{obs}} - 2.5 \log_{10}(1+z)^4 - k(z) - A_{\text{Gal}} \quad (1)$$

where  $z$  is the redshift,  $k(z)$  is the  $k$ -correction and  $A_{\text{Gal}}$  is the interstellar Galactic foreground extinction. The  $k$ -correction was computed for the observed 2dF redshift using the Poggianti (1997) results for the  $b_j$  photographic band, determining the galaxy type from the Madgwick et al. (2002)  $\eta$  parameter. The physical scale length was obtained from the angular scale length using the angular diameter distance computed from the redshift. The mean value of the  $b_j$   $k$ -correction for the emission-line galaxies was  $0.15 \text{ mag}$ . No corrections were made for inclination and internal reddening.

### 3.2 Aperture coverage

We use the surface photometry, discussed in Sec. 3.1 to estimate the fibre covering fraction for the emission line galaxies by measuring the ratio of the light within the fibre aperture, centred on the nucleus, to the total luminosity. Fig. 5 shows the distribution of the covering fraction for the galaxy sample. It shows that the average spectrum in our sample contains 11% of the total flux of the galaxy, with a standard deviation of 6%; the median of the covering fraction distribution is 10%. The average fraction of galaxy light collected by the fibres depends on redshift: the 14% aperture covering fraction for  $z > 0.1$  galaxies is a factor two larger than for  $z < 0.05$  galaxies. Intrinsically brighter galaxies tend to be physically larger than fainter galaxies, but for magnitude-limited survey such as the 2dFGRS they also tend to be found out to larger distances, where fainter galaxies are lost from the sample, so the projected fibre aperture is larger. Thus for a magnitude-limited sample, the fraction of galaxy

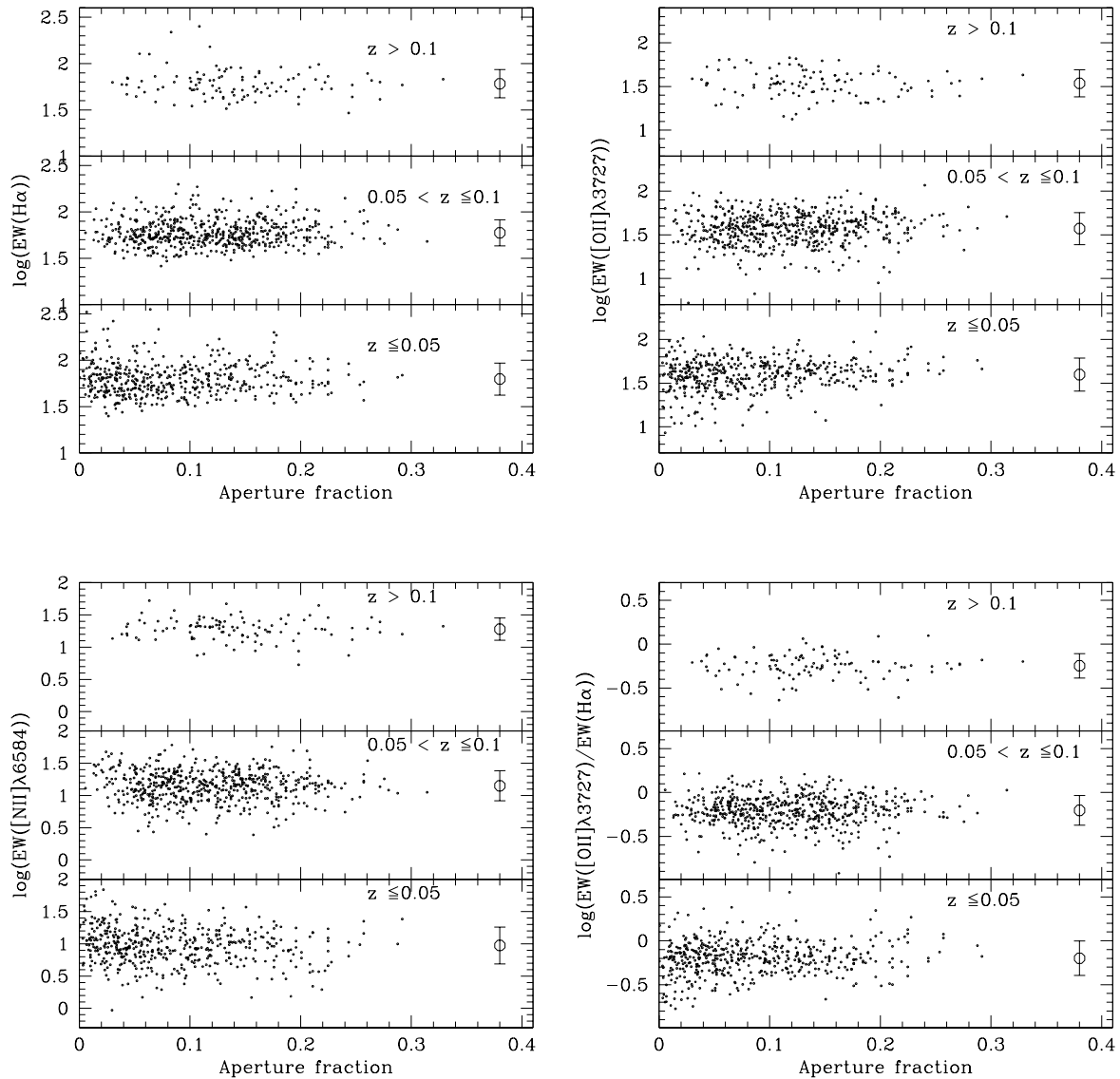


**Figure 6.** A test for aperture effect. Different panels show the relationships between the equivalent widths of  $H\alpha$  (top left),  $[OII]\lambda 3727$  (top right),  $[NII]\lambda 6584$  (bottom left), and the ratio of  $[OII]\lambda 3727$  and  $H\alpha$  equivalent widths (bottom right) and the aperture fraction for the galaxy sample discussed in the paper for different redshift bins. The large circle and the error bar in each panel show the median and the standard deviation of the distribution of emission line equivalent widths and the equivalent width ratio in each redshift bin.

light seen by the fibres is not a strong function of absolute magnitude (see Fig. 9 of Tremonti et al. 2004 for a similar conclusion using a sample of emission line galaxies drawn from the SDSS).

To make sure that the aperture size is not biasing the properties of our galaxy sample, we examine the galaxy properties as a function of the fraction of galaxy light collected through the fibres. Fig. 6 shows the relationship between the aperture fraction and the equivalent width of  $[NII]\lambda 6584$ ,  $[OII]\lambda 3727$ ,  $H\alpha$ , and  $[OII]\lambda 3727/H\alpha$  equivalent width ratio, for different redshift bins. The large open circles and the bars show the medians and the standard deviations of the emission line equivalent width distributions and equivalent width ratio distribution for each redshift bin.

The figure shows that the equivalent widths do not show any sizeable dependence on the fibre covering fraction, independently of redshift. The emission line equivalent widths and equivalent width ratio show no trend with redshift. The distributions of emission line equivalent widths for galaxies with redshifts  $z \geq 0.05$ , a redshift limit recommended by Zaritsky et al. (1995) to minimize the effects of the aperture bias, do not show any trend with the observed fraction of the galaxy light. Consequently, there is no evidence that the properties of our normal emission line galaxy sample are systematically biased. We conclude that the galaxy sample may be used with confidence to study the properties of emission line galaxies.



#### 4 THE [OII] $\lambda$ 3727/H $\alpha$ FLUX RATIO

In this section, we will investigate the sensitivity of [OII] $\lambda$ 3727/H $\alpha$  emission line flux ratio to galaxy and interstellar emitting gas properties.

##### 4.1 Flux calibration and reddening

The relative flux calibration, over the whole spectral coverage of the 2dF spectrograph is uncertain; thus the flux ratio of two distant lines, such as [OII] $\lambda$ 3727 and H $\alpha$ , may not be accurately estimated and may also be subject to systematic errors. Fortunately, using equivalent widths and broad-band photometry, one can accurately estimate the flux ratio. Let us write the emission line equivalent width as a ratio between the emission line flux and the adjacent continuum flux in the observed spectrum, so the extinction-corrected [OII] $\lambda$ 3727/H $\alpha$  emission line flux ratio is given by:

$$I([\text{OII}])/I(\text{H}\alpha) = EW([\text{OII}])/EW(\text{H}\alpha) \times F_{c,[\text{OII}]} / F_{c,\text{H}\alpha} \times 10^{0.4 \times E(B-V)(\kappa([\text{OII}]) - \kappa(\text{H}\alpha))} \quad (2)$$

where  $F_{c,[\text{OII}]}$ , and  $F_{c,\text{H}\alpha}$  are the continuum flux adjacent to [OII] $\lambda$ 3727 and H $\alpha$  respectively,  $E(B - V)$  is the colour excess. We approximate the ratio between the continuum flux by a colour term:  $\log(F_{c,[\text{OII}]} / F_{c,\text{H}\alpha}) = 0.4[z_p - (b_j - R)]$ , where  $z_p = 0.6$ .

The colour excess,  $E(B - V)$ , from obscuration by dust can be estimated from the observed ratio of H $\alpha$  and H $\beta$  line fluxes for each galaxy using the relation:

$$E(B - V) = 1.086\tau_V / R_V \quad (3)$$

where

$$\tau_V = \frac{\ln[F(\text{H}\alpha)/F(\text{H}\beta)] - \ln[I(\text{H}\alpha)/I(\text{H}\beta)]}{\kappa_{\text{H}\alpha} - \kappa_{\text{H}\beta}} \quad (4)$$

$I(\text{H}\alpha)/I(\text{H}\beta)$  is the intrinsic Balmer line flux ratio,  $F(\text{H}\alpha)/F(\text{H}\beta)$  is the observed Balmer line flux ratio,  $\tau_V$  is the effective  $V$ -band optical depth, and  $\kappa_\lambda$  is the optical interstellar extinction curve. We adopt the Milky Way interstellar extinction law of Cardelli, Clayton, & Mathis (1989), with  $R_V = 3.1$ . We make the stellar absorption correction to H $\alpha$ /H $\beta$  flux ratio on a galaxy-by-galaxy basis by fitting Gaussian profiles to both an absorption and emission component for H $\beta$ . We also correct the H $\alpha$ /H $\beta$  flux ratio for Galactic extinction using values taken from Schlegel, Finkbeiner, & Davis (1998) extinction maps. We assume an intrinsic ratio of  $I(\text{H}\alpha)/I(\text{H}\beta) = 2.85$ , corresponding to the case B recombination with a temperature of  $T = 10^4\text{K}$ , and a density of  $n_e \sim 10^2 - 10^4 \text{cm}^{-3}$  (Osterbrock 1989). The different extinction laws available in the literature show similar behaviour in the optical, making the results of our subsequent analysis independent of the chosen extinction law.

Fig. 7 shows the distribution of inferred colour excess for our galaxy sample. The mean  $E(B - V)$  for the galaxies in our sample, after correcting for Galactic extinction, is  $0.34 \pm 0.01$ , and a median of  $0.33 \pm 0.01$ , with a standard deviation of 0.2 magnitude. The mean value found for the galaxy sample is consistent with the widely used average colour excess,  $E(B - V) \sim 0.3$ , for H $\alpha$  measurements of star forming galaxies (e.g., Nakamura et al. 2003, Hopkins et al. 2003, Kewley et al. 2004).

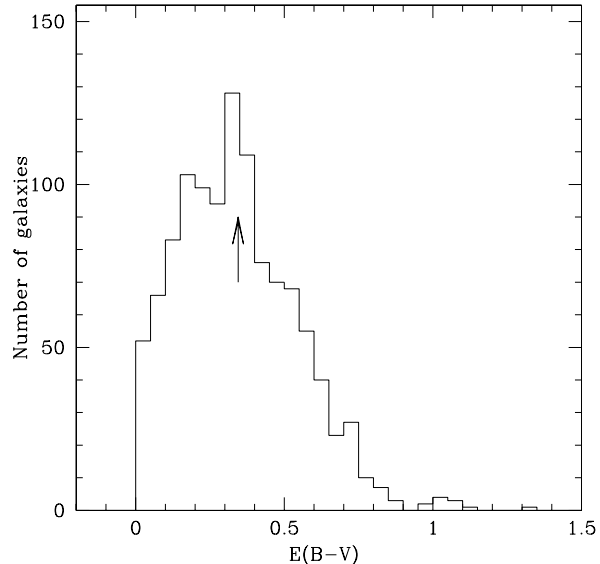


**Figure 7.** Distribution of the colour excess  $E(B - V)$  for the galaxy sample. The vertical arrow shows the location of the mean colour excess for the sample, i.e.,  $E(B - V) = 0.34 \pm 0.01$ .

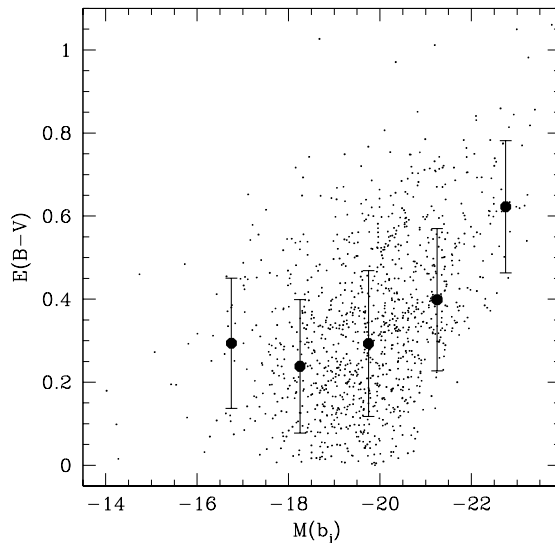


**Figure 8.** Relationship between Balmer-decrement derived colour excess and the absolute magnitude  $M(b_j)$ . Large filled circles and bars show the mean and the standard deviation of the colour excess distributions in 1.5 magnitude wide bins.

Fig. 8 shows the relationship between the colour excess and absolute  $b_j$ -band magnitude. Large filled circles and associated bars show the mean and the standard deviation of the colour excess distributions in 1.5 magnitude wide bins. The Spearman correlation coefficient is  $-0.45$ . The two-sided probability of obtaining this value by chance is almost zero. This indicates that the colour excess and the absolute galaxy magnitude are correlated; i.e., bright galaxies tend to be more affected by internal extinction than faint

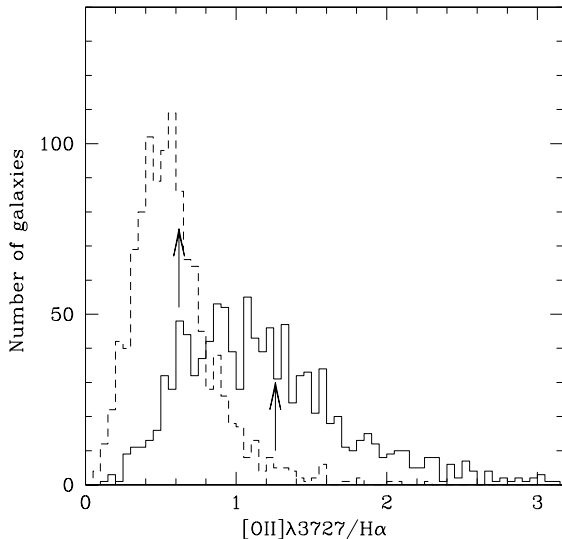


**Figure 9.** Distribution of the  $[\text{OII}]\lambda 3727/\text{H}\alpha$  flux ratio. The continuous line shows the distribution of the extinction-corrected ratio, while the dashed line shows the ratio before extinction correction. The vertical arrows show the means of the extinction-uncorrected and extinction-corrected ratio distributions, i.e.,  $0.62 \pm 0.02$  and  $1.26 \pm 0.03$  respectively.

galaxies, and that there is a large scatter about this trend. The absence of galaxies in the lower right corner of the plot, i.e., the lack of bright galaxies with low colour excess, is unlikely to be due to a selection effect as the selection of sample galaxies was based uniquely on the strength of emission lines compared to the continuum, not on galaxy absolute magnitude and/or emission line ratios. Samples of emission line galaxies selected with different  $\text{H}\beta$  equivalent width cuts between  $10 \text{ \AA}$  and  $20 \text{ \AA}$  do not show a larger zone of exclusion in the lower right corner of Fig. 8.

If the dust were smoothly distributed throughout the galaxies, light from the general stellar population would be obscured, and we would expect to see a lower central surface brightness in galaxies with a larger colour excess. We find no significant correlation between the colour excess and the galaxy central surface brightness or the physical effective radius. This suggests that the obscuring dust in galaxies is not distributed in the same way as the stellar light, it is concentrated close to the sources of line emission (e.g., Stasińska & Sodr e 2001), and/or it has different scale-height to stars.

Fig. 9 shows the distribution of the observed and the extinction-corrected  $[\text{OII}]\lambda 3727/\text{H}\alpha$  emission line flux ratio. The mean value of the extinction-corrected ratio is  $1.26 \pm 0.02$ , compared to  $0.62 \pm 0.02$  of the observed emission line ratio. Both observed and extinction-corrected mean ratios for our emission line galaxy sample are comparable to the same mean ratios for NFGS galaxies (Kewley et al. 2004); this is reasonable since both galaxy samples select roughly similar emission line galaxies. However the observed ratio for our sample is different from the values seen in the UCM galaxy sample (Arag on-Salamanca et al. 2004), and radio-detected galaxies in the First Data Release of the

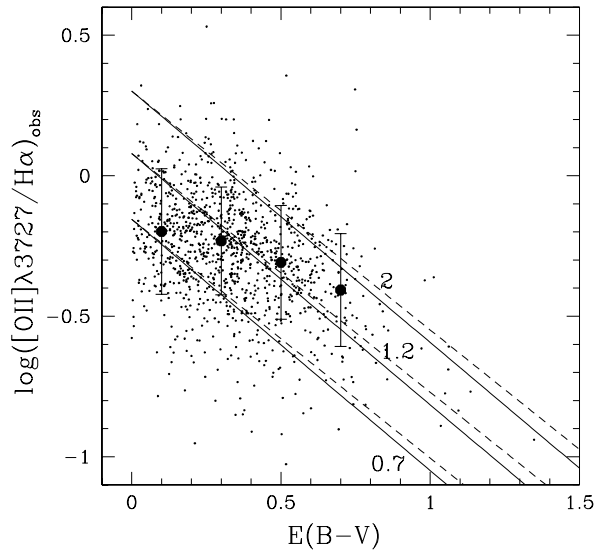


**Figure 10.** The relationship between the colour excess  $E(B-V)$  derived from the Balmer decrement and the observed  $[\text{OII}]\lambda 3727/\text{H}\alpha$  ratio. Large circles and bars show the means and the standard deviations of the observed  $[\text{OII}]\lambda 3727/\text{H}\alpha$  ratio in 0.2 magnitude wide bins. The continuous lines indicate the trend expected from the obscuration curve of Cardelli et al. (1989) for intrinsic  $[\text{OII}]\lambda 3727/\text{H}\alpha$  flux ratios of 0.7, 1.2, and 2.0 from bottom to top, respectively. The dashed lines show the similar trend but using the obscuration curve of Seaton (1979).

SDSS (Hopkins et al. 2003). On the other hand, the mean value of the extinction-corrected ratio is comparable to what is derived for the UCM samples. Note that the Hopkins et al. (2003) sample has the lowest observed mean  $[\text{OII}]\lambda 3727/\text{H}\alpha$  ratio; this is understandable since radio-selected samples tend to be less biased against galaxies with a larger dust content than optically- or  $\text{H}\alpha$ -selected galaxy samples. This confirms the Jansen et al. (2001) finding that an important factor leading to different emission line ratios in different galaxy samples is the sample-dependent mean dust extinction. Thus using  $[\text{OII}]\lambda 3727$  as a star formation rate indicator requires calibration in a reddening-independent way (see also Kewley et al. 2004).

Fig. 10 shows the relationship between internal dust reddening, in terms of colour excess,  $E(B-V)$ , and the logarithm of the observed  $[\text{OII}]\lambda 3727/\text{H}\alpha$  ratio. Large circles and bars show the means and the standard deviations of the observed  $[\text{OII}]\lambda 3727/\text{H}\alpha$  ratio in 0.2 magnitude wide bins. The trend indicated by large solid circles does not change if the medians are used instead of the means. The Spearman correlation coefficient is  $-0.35$ , with the two-sided probability of obtaining this value by chance almost zero, i.e.,  $\sim 8 \times 10^{-32}$ . This indicates a statistically significant correlation between the colour excess,  $E(B-V)$ , and emission line  $[\text{OII}]\lambda 3727/\text{H}\alpha$  flux ratio, consistent with what was found for NFGS galaxies (Jansen et al. 2001; Kewley et al. 2004). We found no convincing relationship between galaxy luminosity and extinction-corrected  $[\text{OII}]\lambda 3727/\text{H}\alpha$  ratio for our galaxy sample, similar to what is observed for UCM galaxies (Arag on-Salamanca et al. 2005, see also Hopkins et al. 2003). However, Jansen et al. (2001) found that after cor-

recting for the internal extinction, a weak correlation still exists between the  $[\text{OII}]\lambda 3727/\text{H}\alpha$  ratio and the galaxy luminosity. They interpret this correlation as an indication of the sensitivity of emission line ratio to gas-phase abundance. If a common extinction law is valid for all the galaxies in the sample, there should be a simple relationship between the observed  $[\text{OII}]\lambda 3727/\text{H}\alpha$  flux ratio and the colour excess. The solid lines in Fig. 10 show the relationships expected using the extinction law of Cardelli et al. (1989) for different values of the intrinsic  $[\text{OII}]\lambda 3727/\text{H}\alpha$  flux ratio. The dashed lines show the expected relationships if the extinction law of Seaton (1979) is used. The fact that the predicted relationship using the Seaton (1979) extinction law is not significantly steeper than what is expected using the extinction law of Cardelli et al. (1989) suggests that the presence or absence of a correlation between absolute magnitude and the extinction-corrected  $[\text{OII}]\lambda 3727/\text{H}\alpha$  is not tied strongly to the adopted extinction law. It is possible that the large scatter of 2dFGRS data may mask a correlation.

#### 4.2 $[\text{OII}]\lambda 3727/\text{H}\alpha$ ratio and metal abundance

To what extent does the systematic variation of galaxy chemical abundance regulate the variation of the  $[\text{OII}]\lambda 3727/\text{H}\alpha$  ratio? Because of the sensitivity of  $[\text{OII}]\lambda 3727$  to metallicity, one may expect that the  $[\text{OII}]\lambda 3727/\text{H}\alpha$  ratio may be related to the metal-content of the star-forming region. Unfortunately, 2dFGRS spectra do not have the required S/N to accurately measure the needed emission lines to estimate electronic temperature-based abundances. Without a reliable electron temperature diagnostic, we have estimated the gas-phase oxygen abundance using the so-called strong emission line method first proposed by Pagel et al. (1979), and extensively used in the literature (e.g., Dopita & Evans 1986, Zaritsky et al. 1994, Contini et al. 2002, Melbourne & Salzer 2002, Pettini et al. 2001, Kobulnicky et al. 2003). This approach is based on the idea that strong lines, i.e.,  $[\text{OII}]\lambda 3727$ ,  $[\text{OIII}]\lambda 4959, \lambda 5007$ , and  $\text{H}\beta$ , contain enough information to get an accurate estimate of the oxygen abundance (McGaugh 1991). This is done through the so-called parameter  $R_{23}$ , introduced by Pagel et al. (1979), and defined as:  $R_{23} = ([\text{OIII}]\lambda 4959, \lambda 5007 + [\text{OII}]\lambda 3727)/\text{H}\beta$ . The  $R_{23}$  parameter is estimated usually from emission line flux ratio. Recently, Kobulnicky & Phillips (2003) have shown that the use of equivalent widths instead of fluxes to derive  $R_{23}$  gives similar results. Due to the limited quality of the relative flux calibration over the whole spectral range covered by the 2dF spectra, we prefer to use the equivalent widths to estimate  $R_{23}$  rather than emission line fluxes.

Fig. 11 shows the relationship between the intrinsic  $[\text{OII}]\lambda 3727/\text{H}\alpha$  flux ratio and the abundance-sensitive  $R_{23}$  parameter. Large filled circles and bars show the means and the standard deviations of logarithmic reddening-corrected  $[\text{OII}]\lambda 3727/\text{H}\alpha$  ratio distributions in 0.15 dex wide bins. The solid line is the linear fit to the NFGS galaxy sample (Jansen et al. 2001). The Spearman correlation coefficient is  $-0.55$ , with the two-sided probability of obtaining this value by chance being almost zero. This indicates that intrinsic  $[\text{OII}]\lambda 3727/\text{H}\alpha$  flux ratio is correlated with the abundance-sensitive  $R_{23}$  parameter with a large statistical significance. The observed correlation does not come as a surprise as the

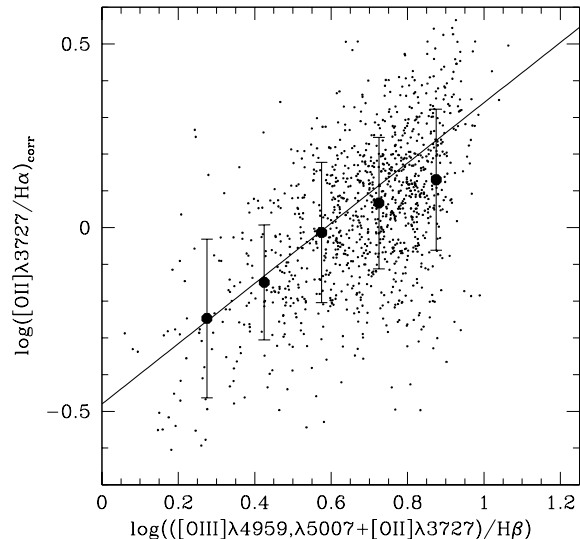


**Figure 11.** The relationship between the reddening-corrected  $[\text{OII}]\lambda 3727/\text{H}\alpha$  ratio and the abundance sensitive  $R_{23}$  parameter. Large filled circles and bars show the means and the standard deviations of logarithmic reddening-corrected  $[\text{OII}]\lambda 3727/\text{H}\alpha$  ratio distributions in 0.15 dex wide bins. The solid line is a linear fit from Jansen et al. (2001).

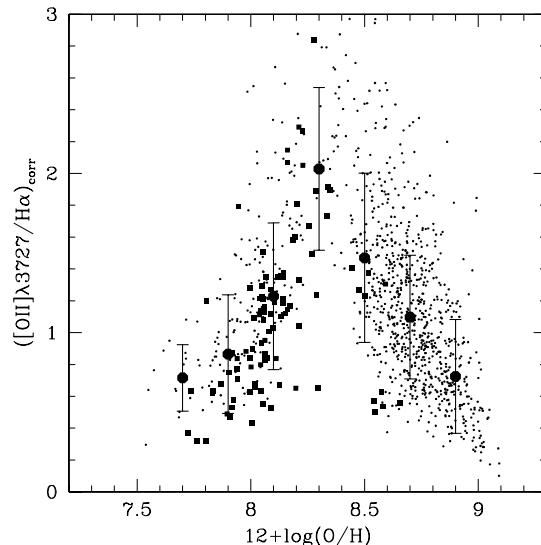


**Figure 12.** The relationship between the reddening-corrected  $[\text{OII}]\lambda 3727/\text{H}\alpha$  ratio and the oxygen abundance in units of  $12 + \log(\text{O}/\text{H})$ . The abundances are calculated using the McGaugh (1991) calibration of the  $R_{23}$  method (see text for more details). Filled circles and associated error bars show the means and the standard deviations of  $[\text{OII}]\lambda 3727/\text{H}\alpha$  ratio distributions as a function of oxygen abundance in 0.2 dex wide bins. Filled squares show galaxies with high ionization-sensitive ratios, i.e.,  $\log([\text{OIII}]\lambda 5007/\text{H}\beta) \geq 0.5$ . These galaxies tend to have, at a given oxygen abundance, lower reddening-corrected  $[\text{OII}]\lambda 3727/\text{H}\alpha$  ratios than galaxies with low and intermediate  $\log([\text{OIII}]\lambda 5007/\text{H}\beta)$  ratios (see text for more details).

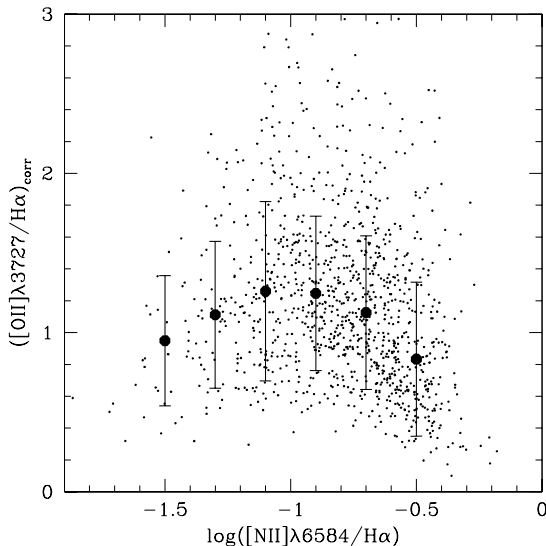


**Figure 13.** The relationship between the reddening-corrected  $[\text{OII}]\lambda 3727/\text{H}\alpha$  ratio and the abundance sensitive emission line ratio  $[\text{NII}]\lambda 6584/\text{H}\alpha$ . Filled circles and associated error bars show the means and the standard deviations of  $[\text{OII}]\lambda 3727/\text{H}\alpha$  ratio distributions in 0.2 dex wide bins.

variation of the  $R_{23}$  parameter is related to the variation of both the  $[\text{OII}]\lambda 3727/\text{H}\alpha$  ratio, and the ionization conditions as traced by the ratio of two different oxygen emission lines, i.e.,  $\log R_{23} \propto \log([\text{OII}]\lambda 3727/\text{H}\alpha) + \log(1 + \text{O}_{32})$ , where  $\text{O}_{32} = [\text{OIII}]\lambda 4959, \lambda 5007/[\text{OII}]\lambda 3727$  is an ionization-sensitive ratio.

The dependence of the abundance-sensitive  $R_{23}$  parameter on the metallicity is degenerate. Indeed, at a fixed value of  $R_{23}$  two different values of metallicity are possible: at the same oxygen abundance, different ionization parameters lead to different values of  $R_{23}$  (McCall et al. 1985). Different techniques have been developed to break this degeneracy with some success (Alloin et al. 1979; McGaugh 1991, van Zee et al. 1998, Kobulnicky et al. 1999). To estimate the oxygen abundance we have used the calibration of McGaugh (1991). This calibration is parameterized as a function of the excitation-sensitive parameter  $\text{O}_{32}$ . We have used the secondary metallicity indicator  $[\text{NII}]\lambda 6583/\text{H}\alpha$  to determine which branch of the McGaugh calibration to use (see Lamareille et al. 2004 for a detailed discussion of the abundance estimate for the galaxy sample).

Fig. 12 shows the relationship between oxygen abundance, expressed in terms of  $12 + \log(\text{O}/\text{H})$ , and the extinction-corrected  $[\text{OII}]\lambda 3727/\text{H}\alpha$  ratio. Large filled circles and the associated bars show the means and the standard deviations of the  $[\text{OII}]\lambda 3727/\text{H}\alpha$  ratio distributions in 0.2 dex wide bins. The relationship between the extinction-corrected  $[\text{OII}]\lambda 3727/\text{H}\alpha$  ratio and oxygen abundance splits into two regimes. For metal-poor galaxies, i.e.,  $12 + \log(\text{O}/\text{H}) \lesssim 8.4$ , the intrinsic  $[\text{OII}]\lambda 3727/\text{H}\alpha$  flux ratio increases with oxygen abundance. For these galaxies, the Spearman rank correlation coefficient is 0.73, with a two-sided probability of obtaining this value by chance almost equal to zero, i.e.,  $2.5 \times 10^{-51}$ . This indicates a strong corre-

lation between the extinction-corrected  $[\text{OII}]\lambda 3727/\text{H}\alpha$  ratio and oxygen abundance for metal-poor galaxies. On the other hand, metal-rich galaxies, i.e.,  $12 + \log(\text{O}/\text{H}) \gtrsim 8.4$ , show a similar trend but with a slope of the opposite sign. The Spearman rank correlation coefficient is  $-0.6$ , with a two-sided probability of obtaining this value by chance almost equal to zero, i.e.,  $2.5 \times 10^{-33}$ , suggesting a strong anti-correlation between the intrinsic  $[\text{OII}]\lambda 3727/\text{H}\alpha$  flux ratio and oxygen abundance. The metal-rich branch in the  $[\text{OII}]\lambda 3727/\text{H}\alpha$  vs.  $12 + \log(\text{O}/\text{H})$  diagram is consistent with the same relationship for the NFGS galaxy sample constructed by Kewley et al. (2004) using the McGaugh (1991) calibration.

However, there is a concern here. Because radial abundance gradients are known to exist in spiral galaxies, it has been argued, depending on the metallicity gradients and the relative weight of different HII regions in the integrated emission line spectra, that the  $R_{23}$  parameter might not be a useful indicator of galaxy overall metallicity (Stasińska & Sodr e 2001; but see Kobulnicky et al. 1999 for a different view). To establish the dependence of  $[\text{OII}]\lambda 3727/\text{H}\alpha$  flux ratio on the emitting gas metallicity, it is useful to confirm the observed correlation in Fig 12 using metallicity indicators other than the  $R_{23}$  parameter. The  $[\text{NII}]\lambda 6584/\text{H}\alpha$  ratio has been proposed recently as an empirical metallicity indicator (van Zee et al. 1998, Denicol o et al. 2002). The  $[\text{NII}]\lambda 6584/\text{H}\alpha$  ratio is less sensitive to the electron temperature than the  $R_{23}$  parameter, making this ratio less affected by the doubled value problem (e.g., Kewley & Dopita 2002). A valuable advantage of using this emission line ratio is its independence of both reddening and the accuracy of the relative flux calibration. In integrated spectra of galaxies, one expects however a non negligible contribution from a diffuse medium (e.g., Collins et al. 2000; Zurita et al. 2000). The  $[\text{NII}]\lambda 6584/\text{H}\alpha$  ratios in the diffuse medium are generally larger than in nearby HII regions. The effect of the diffuse medium is to increase the  $[\text{NII}]\lambda 6584/\text{H}\alpha$  ratio by about 30% at most: this increase is smaller than the metallicity dependence of this ratio, making the ratio a useful metallicity indicator (see Stasińska & Sodr e 2001, and references therein). It is worth mentioning that our sample galaxies are distributed along a well defined sequence in the  $[\text{NII}]\lambda 6584/\text{H}\alpha$  ratio against  $R_{23}$  parameter diagram, interpreted as a metallicity-excitation sequence, similar to the sequence defined by local HII galaxies (Fig. 14c of McCall et al. 1985). Another proposed empirical metallicity indicator that does not suffer from the double value problem is the  $[\text{NII}]\lambda 6584/[\text{OII}]\lambda 3727$  ratio (Dopita et al. 2000, Kewley & Dopita 2002). It is however strongly dependent on the extinction correction, and the spectrophotometric accuracy of the spectra.

Fig. 13 shows the relationship between the extinction-corrected  $[\text{OII}]\lambda 3727/\text{H}\alpha$  ratio and the  $[\text{NII}]\lambda 6584/\text{H}\alpha$  ratio. Filled circles and associated bars show the means and the standard deviations of the  $[\text{OII}]\lambda 3727/\text{H}\alpha$  ratio in 0.2 dex wide bins. For galaxies with  $\log([\text{NII}]\lambda 6584/\text{H}\alpha) \gtrsim -1$ , corresponding roughly to  $\log(\text{O}/\text{H}) + 12 \gtrsim 8.4$  using the van Zee et al. (1998) calibration, the Spearman correlation coefficient is  $-0.36$ , with the two-sided probability of obtaining this value by chance of  $9 \times 10^{-27}$ . This indicates a statistically significant anti-correlation between the metallicity indicator and the extinction-corrected  $[\text{OII}]\lambda 3727/\text{H}\alpha$



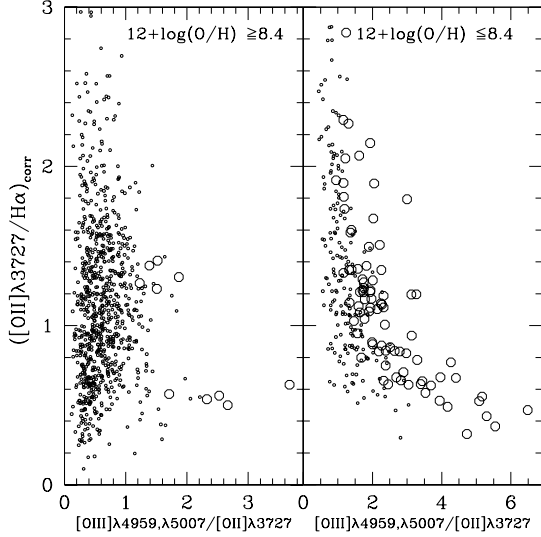


**Figure 15.** Left: the relationship between ionization parameter sensitive  $[\text{OIII}]\lambda 4959\lambda 5007/[\text{OII}]\lambda 3727$  and the  $[\text{OII}]\lambda 3727/\text{H}\alpha$  ratio for metal-rich galaxies ( $12 + \log(\text{O}/\text{H}) \geq 8.4$ ). Right: similar to the left panel but for metal-poor galaxies ( $12 + \log(\text{O}/\text{H}) \leq 8.4$ ). Large circles show galaxies with  $\log([\text{OIII}]\lambda 5007/\text{H}\beta) \geq 0.5$ .

ratio. For metal-rich galaxies, i.e.,  $\log(\text{O}/\text{H}) + 12 \gtrsim 8.4$ , nitrogen is thought to be predominantly a secondary element (e.g., Villa-Costas & Edmunds 1993, Henry et al. 2000), so the observed trend reflects the sensitivity of the intrinsic  $[\text{OII}]\lambda 3727/\text{H}\alpha$  ratio to abundance within this metallicity regime. For galaxies with low  $[\text{NII}]\lambda 6584/\text{H}\alpha$  ratio, i.e., mainly metal-poor galaxies for which nitrogen is a primary element (Matteucci 1986), the relationship between  $[\text{NII}]\lambda 6584/\text{H}\alpha$  and the extinction-corrected  $[\text{OII}]\lambda 3727/\text{H}\alpha$  flux ratio is reversed. The Spearman correlation coefficient is 0.33, with the two-sided probability of obtaining this value by chance of  $1.3 \times 10^{-8}$ . This indicates a statistically significant correlation between the metallicity indicator and the extinction-corrected  $[\text{OII}]\lambda 3727/\text{H}\alpha$  flux ratio for metal-poor galaxies. This confirms that the variation of extinction-corrected  $[\text{OII}]\lambda 3727/\text{H}\alpha$  ratio is coupled with the evolution of metallicity.

### 4.3 $[\text{OII}]\lambda 3727/\text{H}\alpha$ ratio and excitation state

Kewley et al. (2004) have found that for  $12 + \log(\text{O}/\text{H}) \gtrsim 8.5$ , the variation of extinction-corrected  $[\text{OII}]\lambda 3727/\text{H}\alpha$  flux ratio does not depend on the ionization state of interstellar emitting gas. For our galaxy sample, the scatter of the extinction-corrected  $[\text{OII}]\lambda 3727/\text{H}\alpha$  flux ratio at a given metallicity appears to be related to the variation of the ionization parameter in galaxies. Indeed, at a given oxygen abundance, galaxies with large ionization-sensitive  $[\text{OIII}]\lambda 5007/\text{H}\beta$  ratio, shown as filled squares in Fig. 12, tend to have lower intrinsic  $[\text{OII}]\lambda 3727/\text{H}\alpha$  flux ratio than galaxies with a low-to-intermediate ionization-sensitive ratio. This suggests that the variation of the excitation state of the interstellar emitting gas in galaxies may contribute to the observed variation of the  $[\text{OII}]\lambda 3727/\text{H}\alpha$  ratio.

The left panel of Fig. 14 shows the diagnostic diagram of  $[\text{OII}]\lambda 3727/\text{H}\beta$  ratio as a function of  $[\text{OIII}]\lambda 4959, \lambda 5007/\text{H}\beta$  for our galaxy sample. Large/small circles show metal-poor/metal-rich galaxies, i.e.,  $12 + \log(\text{O}/\text{H}) \leq 8.4 (> 8.4)$ . The continuous line shows the theoretical sequence of McCall, Rybski, & Shields (1985) for line ratios of HII galaxies as a function of metallicity. Along the track, the metallicity is high at the lower left, i.e., for low excitation systems, and low at the upper right, i.e., for high excitation systems (McCall et al. 1985). Most of the metal-poor galaxies in the sample lie in the moderate- to high-excitation regime populated by local HII galaxies, i.e.,  $\log([\text{OIII}]\lambda 5007/\text{H}\beta) \geq 0.3$ , while metal-rich galaxies are located in the low-excitation regime. The right panel of Fig. 14 shows the  $[\text{OIII}]\lambda 5007/\text{H}\beta$  ratio versus the absolute  $b_j$ -band magnitude for our sample galaxies. The galaxies define a continuous sequence in this diagram. The observed sequence is interpreted as being a variation in the metallicity of the ionized gas (Dopita & Evans 1986; Stasińska 1990). On average faint/metal-poor galaxies tend to be highly ionized, while bright/metal-rich galaxies are characterized by low-ionization parameters.

The line ratio  $\text{O}_{32}$  is a function of both ionization parameter and metallicity (Kewley & Dopita 2002). For a galaxy sample that covers a large range of metallicity, a given  $\text{O}_{32}$  could correspond to different combinations of abundances and ionization parameters. In order to distinguish between the effects of ionization and metallicity, we have split the galaxy sample into metal-rich, i.e.,  $12 + \log(\text{O}/\text{H}) > 8.4$ , and metal-poor, i.e.,  $12 + \log(\text{O}/\text{H}) \leq 8.4$ , galaxy subsamples. Fig. 15 shows the extinction-corrected  $[\text{OII}]\lambda 3727/\text{H}\alpha$  flux ratio versus  $\text{O}_{32}$  ratio for metal-rich and metal-poor subsamples respectively. The  $\text{O}_{32}$  ratio has been estimated using emission line equivalent widths. Kobulnicky & Phillips (2003) have shown that estimates of this ratio using equivalent widths give results similar to using emission line fluxes. Large circles show galaxies with  $\log([\text{OIII}]\lambda 5007/\text{H}\beta) \geq 0.5$ . Note that for the metallicity range covered by galaxies in our sample, the  $[\text{OIII}]\lambda 5007/\text{H}\beta$  ratio is sensitive mainly to ionization parameter, and is almost independent of metallicity (Kewley et al. 2004).

For metal-rich galaxies, the Spearman correlation coefficient for the relationship between extinction-corrected  $[\text{OII}]\lambda 3727/\text{H}\alpha$  ratio and  $\text{O}_{32}$  ratio is 0.07, with the two-sided probability of obtaining this value by chance of 0.05. This indicates that there is no statistically significant correlation between the intrinsic  $[\text{OII}]\lambda 3727/\text{H}\alpha$  flux ratio and the ionization-sensitive  $\text{O}_{32}$  ratio, in agreement with the Kewley et al. (2004) result. The subsample of metal-rich galaxies spans a limited range in ionization-sensitive ratio; the distribution of  $\text{O}_{32}$  ratio for metal-rich galaxies has a mean of 0.63, with an accuracy of 0.01, and 70% of the galaxies of this subsample with a ratio less than 0.5. The low  $\text{O}_{32}$  ratio suggests that for metal-rich galaxies, a significant fraction of oxygen emission results from  $\text{O}^+$  species.

Metal-poor galaxies exhibit a larger range of ionization-sensitive diagnostic ratios, extending to extreme excitation states. The majority of galaxies in our sample with large excitation-sensitive ratios are metal-poor. The distribution of the  $\text{O}_{32}$  ratio for metal-poor galaxies has a mean of  $1.66 \pm 0.07$ , with 72% of the galaxies having  $\text{O}_{32}$  larger than unity.

Metal-poor galaxies with low to moderate excitation, i.e.,  $\log([\text{OIII}]\lambda 5007/\text{H}\beta) < 0.5$  cover a wide range



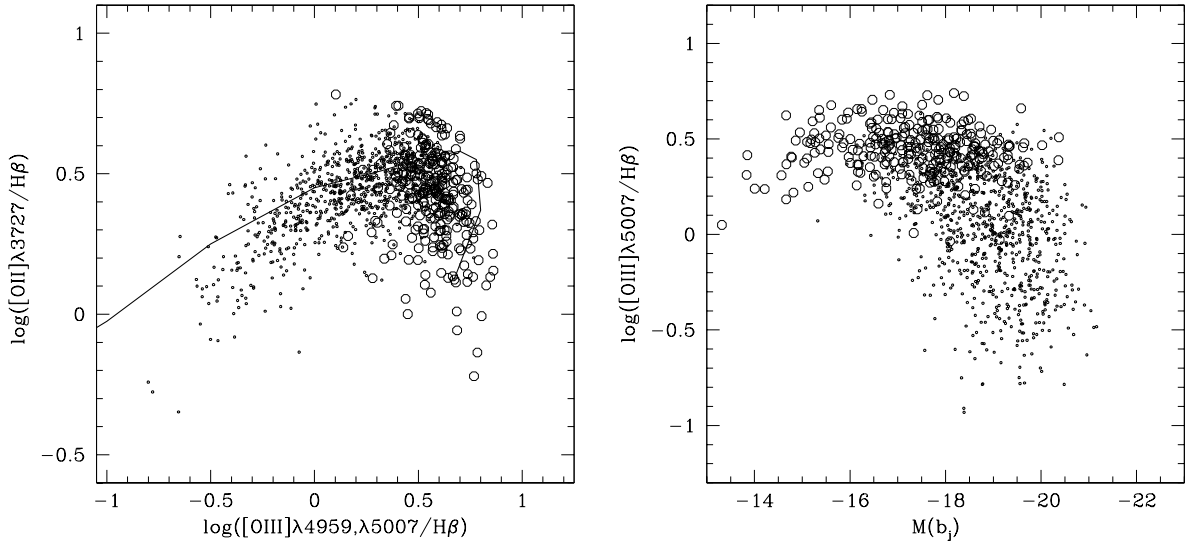


**Figure 14.** Left: The relationship between  $[\text{OII}]\lambda 3727/\text{H}\beta$  and  $[\text{OIII}]\lambda 4959, \lambda 5007/\text{H}\beta$  for our sample galaxies. Large (small) circles show metal-poor (metal-rich) galaxies ( $12 + \log(O/H) \leq 8.4$  [ $> 8.4$ ]). The solid line shows the theoretical sequence from McCall et al. (1985), which fit the local HII galaxies with metallicity decreasing from the left to the right. Right: Excitation sensitive ratio versus  $b_j$ -band absolute magnitude for our sample galaxies.

in ionization-sensitive diagnostic ratios, i.e.,  $0.2 \lesssim \text{O}_{32} \lesssim 3$ , with a mean of  $1.23 \pm 0.04$ . For these galaxies, the Spearman correlation coefficient for the relationship between extinction-corrected  $[\text{OII}]\lambda 3727/\text{H}\alpha$  ratio and  $\text{O}_{32}$  ratio is  $-0.67$ , with a two-sided probability of obtaining this value by chance of  $1.1 \times 10^{-25}$ . This indicates a statistically significant anti-correlation between the intrinsic  $[\text{OII}]\lambda 3727/\text{H}\alpha$  flux ratio and the ionization-sensitive  $\text{O}_{32}$  ratio. Highly ionized metal-poor galaxies, i.e.,  $\log([\text{OIII}]\lambda 5007/\text{H}\beta) \geq 0.5$ , span a large range of ionization parameter, i.e.,  $1 \lesssim \text{O}_{32} \lesssim 10$ , with a mean ratio of  $2.59 \pm 0.16$ . These galaxies show a stronger anticorrelation between the extinction-corrected  $[\text{OII}]\lambda 3727/\text{H}\alpha$  flux ratio and the ionization-sensitive  $\text{O}_{32}$  ratio: the Spearman correlation coefficient for these galaxies is  $-0.8$ , with the two-sided probability of obtaining this value by chance of  $2.4 \times 10^{-18}$ .

The lack of a dependence of the extinction-corrected  $[\text{OII}]\lambda 3727/\text{H}\alpha$  ratio on ionization state of the interstellar medium for NFGS galaxies may be attributed to the absence of such highly ionized metal-poor galaxies. This galaxy sample consists mostly of normal star-forming galaxies, with few active starburst galaxies and extremely metal-poor dwarfs (Jansen et al. 2000). The observed dependence of extinction-corrected  $[\text{OII}]\lambda 3727/\text{H}\alpha$  flux ratio on ionization state of the interstellar medium for metal-poor and highly ionized galaxies suggests that at low metallicity, where the electronic temperature is very high, a significant fraction of oxygen atoms may be in the form of  $\text{O}^{++}$  and higher excitation levels. For metal-poor galaxies with a high ionization parameter, the variation of the extinction-corrected  $[\text{OII}]\lambda 3727/\text{H}\alpha$  ratio is regulated by the variation of the ionization parameter rather than metallicity. Fig. 16 shows the distributions of  $\text{H}\alpha$  and  $[\text{OII}]\lambda 3727$  emission line equivalent widths, oxygen abundance, and  $b_j$ -band absolute magnitude for galaxies with  $\log([\text{OIII}]\lambda 5007/\text{H}\beta) \geq 0.5$ . The highly ionized galaxy pop-

ulation in our sample, for which a strong anti-correlation is observed between the extinction-corrected  $[\text{OII}]\lambda 3727/\text{H}\alpha$  flux ratio and the excitation-sensitive ratio  $\text{O}_{32}$ , consists mainly of faint metal-poor galaxies, in which the starburst is still vigorously active, keeping the high ionization conditions. An important conclusion regarding the high ionization galaxy population is that the estimate of their star formation rate based on the  $[\text{OII}]\lambda 3727$  luminosity may be significantly underestimated, even when the dependence of the extinction-corrected  $[\text{OII}]\lambda 3727/\text{H}\alpha$  ratio on metallicity is corrected. Guzmán et al. (1997) have shown that for a  $z = 0.137$  compact field galaxy with extreme ionization-sensitive ratios, i.e.,  $\text{O}_{32} = 3.8$  and  $[\text{OIII}]\lambda 5007/\text{H}\beta = 5.27$ , the star formation rate based on  $[\text{OII}]\lambda 3727$  luminosity is underestimated by a factor of 6, compared to the star formation rate based on  $\text{H}\alpha$  luminosity.

## 5 SUMMARY AND CONCLUSIONS

We have used spectrophotometric data for a sample of 1 124 nearby star-forming galaxies from the 2dFGRS sample, spanning a range of 7 magnitudes in  $M(b_j)$ , to investigate the systematic variation of the  $[\text{OII}]\lambda 3727/\text{H}\alpha$  emission-line ratio as a function of galaxy and interstellar emitting gas properties.

The 2dF fibres cover, on average, about 11% of the total light of the galaxy. No evidence for systematic aperture bias affecting the estimate of the emission line properties is found. This suggests that our spectra are sufficiently representative of the integrated galaxy spectra. The nebular extinction as derived from the Balmer decrement is found to correlate with the intrinsic absolute luminosity. The mean of the distribution of the extinction-corrected emission line  $[\text{OII}]\lambda 3727/\text{H}\alpha$  flux ratio is similar to what was found for

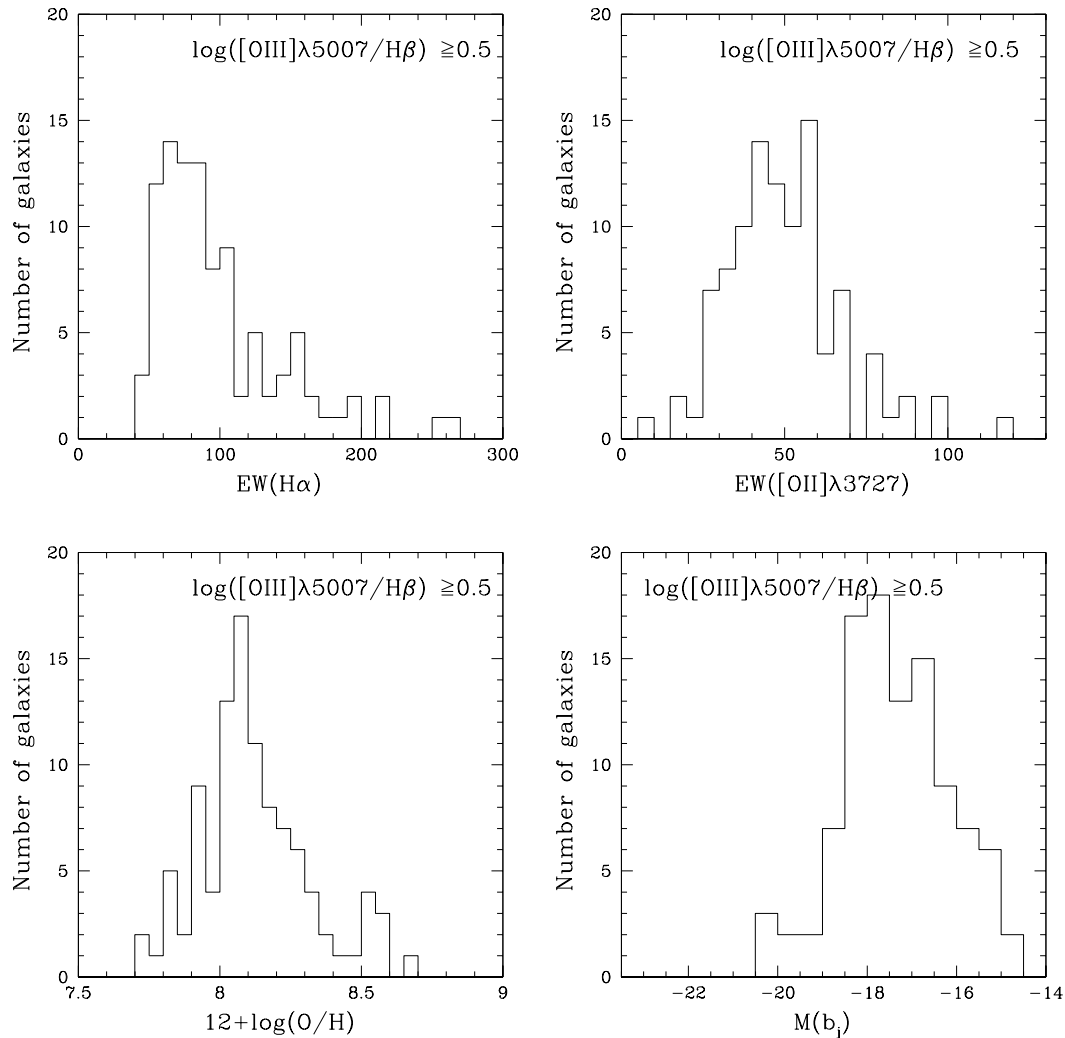


**Figure 16.** Distribution of properties of highly ionized galaxies, i.e.,  $\log([\text{OIII}]\lambda 5007/\text{H}\beta) \geq 0.5$ . The upper panels show the equivalent widths of  $[\text{OII}]\lambda 3727$  and  $\text{H}\alpha$  emission lines, with medians of  $85 \text{ \AA}$  and  $48 \text{ \AA}$  respectively. The lower panels show the distributions of oxygen abundance and absolute  $b_j$ -band magnitude. The median of oxygen abundance distribution is  $12 + \log(\text{O}/\text{H}) = 8.1$  ( $\sim Z_{\odot}/4$ ), and  $-17.4$  for  $b_j$ -band magnitude distribution.

other galaxy samples, selected in different ways, confirming that the internal reddening is a driver behind the variation of the observed  $[\text{OII}]\lambda 3727/\text{H}\alpha$ .

We confirm that there is a strong correlation between the extinction-corrected  $[\text{OII}]\lambda 3727/\text{H}\alpha$  ratio and the oxygen abundance for metal-rich galaxies, and extend the observed correlation further to the metal-poor regime, i.e.,  $12 + \log(\text{O}/\text{H}) \lesssim 8.4$ . This relationship consists of two branches, i.e., where the  $[\text{OII}]\lambda 3727/\text{H}\alpha$  ratio is increasing (decreasing) as a function of the oxygen abundance for  $12 + \log(\text{O}/\text{H}) \lesssim 8.4$  ( $\gtrsim 8.4$ ). For metal-rich galaxies, there is no clear dependence of the extinction-corrected  $[\text{OII}]\lambda 3727/\text{H}\alpha$  ratio on the ionization parameter, in agreement with what was reported for NFGS sample galaxies. However, a strong correlation is seen for metal-poor galaxies, especially for those with high ionization-sensitive ratios. These galaxies tend to be faint and strong  $[\text{OII}]\lambda 3727$  emitters. For these galaxies, the  $[\text{OII}]\lambda 3727/\text{H}\alpha$  ratio is more

sensitive to the variation of ionization parameter than to the variation of oxygen abundance.

An emission-line galaxy spectrum is the result of many physical properties of the ionized gas, e.g., the chemical abundance and dust content, and of the relative importance of the ongoing star-forming activity, e.g., the star formation timescale. The excitation state depends both on the emitting gas abundance and on the ionizing stellar flux, which in turn depends on the effective temperature of the ionizing stars, which depends on the stellar initial metallicity, and on the age of the ongoing star formation event. Different detection techniques preferentially detect emission line galaxies at different stages of the starburst. An important conclusion is that using the  $[\text{OII}]\lambda 3727$  emission line as a star formation rate indicator requires a good understanding of the selection criteria of the galaxy sample under investigation, and how they determine its properties, i.e., extinction, metallicity, and excitation state.

**ACKNOWLEDGEMENTS**

M. M. would like to thank warmly A. Aragón-Salamanca for highlighting discussions, and sharing his results prior to publication. We thank an anonymous referee for useful comments which significantly improved our paper.

**REFERENCES**

- Abazajian K., et al., 2003, *AJ*, 126, 2081  
 Alloin D., Collin-Souffrin S., Joly M., Vigroux L., 1979, *A&A*, 78, 200  
 Baldwin J.A., Phillips M.M., Terlevich R., 1981, *PASP*, 93, 5  
 Bertin E., 1998, *SEtractor User's Guide*, Institut d'Astrophysique de Paris  
 Bertin E., Arnouts S., 1996, *A&AS*, 117, 396  
 Broadhurst T.J., Ellis R.S., Shanks T., 1988, *MNRAS*, 235, 827  
 Cardelli J.A., Clayton G.C., Mathis J.S., 1989, *ApJ*, 329, 33  
 Carter B.J., Fabricant D.G., Geller M.J., Kurtz M.J., McLean B., 2001, *ApJ*, 559, 606  
 Colless M., Ellis R.S., Taylor K., Hook R.N., 1990, *MNRAS*, 244, 408  
 Colless M., Dalton G., Maddox S.J., et al., 2001, *MNRAS*, 328, 1039  
 Collins J.A., Rand R.J., Duric N., & Waltherbos R.A.M., 2000, *ApJ*, 536, 645  
 Contini T., Treyer M.A., Sullivan M., Ellis R.S., 2002, *MNRAS*, 330, 75  
 Cowie L.L., Hu E.M., Songaila A., Egami E., 1997, *ApJ*, 481, L9  
 Cross N., Driver S.P., Couch W., et al., 2001, *MNRAS*, 324, 825  
 Denicoló G., Terlevich R., Terlevich E., 2002, *MNRAS*, 330, 69  
 Dopita M.A., Evans I.N., 1986, *ApJ*, 307, 431  
 Dopita M.A., Kewley L.J., Heisler C.A., & Sutherland R.S., 2000, *ApJ*, 542, 224  
 Gallagher J.S., Bushouse H., Hunter D.A., 1989, *ApJ*, 97, 700  
 Gavazzi G., Zaccardo A., Sanvito G., Boselli A., Bonfanti C., 2004, *A&A*, 417, 499  
 Gil de Paz A., Aragón-Salamanca A., Gallego J., et al., 2000, *MNRAS*, 316, 357  
 Guzmán R., Gallego J., Koo D.C., et al. 1997, *ApJ*, 489, 559  
 Hambly N. C., McGillivray H. T., Read M. A., et al., 2001, *MNRAS*, 326, 1279  
 Hambly N. C., Irwin M. J., McGillivray H. T., 2001, *MNRAS*, 326, 1295  
 Hammer F., Flores H., Lilly S.J., et al., 1997, *ApJ*, 481, 49  
 Henry R.B.C., Edmunds M.G., Köppen J., *ApJ*, 197, 7608  
 Hippelein H., Maier C., Meisenheimer K., et al., 2003, *A&A*, 402, 65  
 Hogg D.W., Cohen J.G., Blandford R., Pahre M.A., 1998, *ApJ*, 504, 622  
 Hopkins A.M., Miller C.J., Nichol R.C., et al., 2003, *ApJ*, 599, 971  
 Jansen R.A., Franx M., Fabricant D., 2001, *ApJ*, 551, 825  
 Jansen R.A., Franx M., Fabricant D., Caldwell N., 2000, *ApJS*, 126, 331  
 Kauffmann G., Keckman T.M., Tremonti C., et al., 2003, *MNRAS*, 346, 1055  
 Kennicutt R.C., 1992, *ApJ*, 388, 310  
 Kewley L.J., Heisler C.A., Dopita M.A., Lumsden S., 2001, *ApJS*, 132, 37  
 Kewley L.J., Dopita M.A., 2002, *ApJS*, 142, 35  
 Kewley L.J., Geller M.J., Jansen R.A., 2004, *AJ*, 127, 2002  
 Kobulnicky H. A., Kennicutt Jr. R. C., Pizagno J. L., 1999, *ApJ*, 514, 544  
 Kobulnicky H. A., Phillips A. C., 2003, *ApJ*, 599, 1031  
 Kobulnicky H. A., Willmer C. N. A., Phillips A. C., 2003, *ApJ*, 599, 1006  
 Kochanek C.S., Pahre M.A., Falco E.E., submitted (*astro-ph/0011458*)  
 Kong X., Cheng F.Z., Weiss A., Charlot S., 2002, *A&A*, 396, 503  
 Lamareille F., Mouhcine M., Contini T., Lewis I.J., Maddox S.J., 2004, *MNRAS*, 350, 396  
 Lewis I.J., Cannon R.D., Taylor K., et al., 2002a, *MNRAS* 333, 279  
 Lewis I.J., Balogh M., De Propris R., et al., 2002b, *MNRAS*, 334, 673  
 Lilly S.J., Le Fèvre O., Hammer F., Crampton D., 1996, *ApJ*, 460, 1  
 Madau, P., Ferguson, H.C., Dickinson, M.E., et al., 1996, *MNRAS*, 283, 1388  
 Maddox S. J., Efstathiou G., Sutherland W. J., Loveday J., 1990a, *MNRAS*, 243, 692  
 Maddox S. J., Efstathiou G., Sutherland W. J., 1990b, *MNRAS*, 246, 433  
 Madgwick, D.S., Lahav, O., Baldry, I.K., et al., 2002, *MNRAS*, 333, 133  
 Matteucci F., 1986, *MNRAS*, 221, 911  
 McCall M.L., Rybski P.M., Shields G.A., 1985, *ApJS*, 57, 1  
 McGaugh S. S., 1991, *ApJ*, 380, 140  
 Melbourne J., Salzer J. J., 2002, *AJ*, 123, 2302  
 Nakamura O., Fukugita M., Brinkmann J., Schneider D.P., 2004, *AJ*, 127, 2511  
 Osterbrock D.E., 1989, *Astrophysics of Gaseous Nebulae and Active Galactic Nuclei (Mill Valley: Unvi. Sci.)*  
 Pagel B.E.J., Edmunds M.G., Blackwell D.E., Chum M.S., Smith G., 1979, *MNRAS*, 189, 95  
 Pettini M., Shapley A. E., Steidel C. C., et al., 2001, *ApJ*, 554, 981  
 Poggianti B.M., 1997, *A&AS*, 122, 399  
 Rosa-González D., Terlevich E., Terlevich R., 2002, *MNRAS*, 332, 283  
 Salzer J.J., MacAlpine G.M., Boroson T.A., 1989, *ApJS*, 70, 479  
 Salzer J.J., Gronwall C., Lipovetsky V.A., et al., 2000, *AJ*, 120, 80  
 Schlegel D.J., Finkbeiner D.P., Davis M., 1998, *ApJ*, 500, 525  
 Shao Z., Maddox S. J, Jones J. B. & Coles P., 2003, *MNRAS*, 338, 72  
 Spergel D.N., et al., 2003, *ApJS*, 148, 175  
 Stasińska G., 1990, *A&AS*, 83, 501  
 Stasińska G., Sodr  L., 2001, *A&A*, 374, 919  
 Stoughton C., Lupton R.H., Bernardi M., et al. 2002, *AJ*, 123, 486  
 Thompson D.J., Djorgovski S., 1991, *ApJ*, 371, 55  
 Tremonti C.A., Heckman T.M., Kauffmann G., et al., 2004, *ApJ*, 613, 898  
 Tresse L., Maddox S.J., Loveday J., Singleton C., 1999, *MNRAS* 310, 262  
 Tresse L., Maddox S.J., Le Fèvre O., Cuby J.-G., 2002, *MNRAS*, 337, 369  
 van Zee L., Salzer J.J., Haynes M.P., O'Donoghue A.A., Balonek T.J., 1998, *AJ*, 116, 2805  
 Veilleux S., Osterbrock D. E., 1987, *ApJS*, 63, 295  
 Vila Costas M.B., Edmunds M.G., 1993, *MNRAS*, 265, 199  
 Zaritsky D., Kennicutt R.C Jr., Huchra J.P., 1994, *ApJ*, 420, 87  
 Zaritsky D., Zabludoff A.I., Willick J.A., 1995, *AJ*, 110, 1602  
 Zurita A., Rozas M., & Beckman J.E., 2000, *A&A*, 363, 9

This paper has been produced using the Royal Astronomical Society/Blackwell Science L<sup>A</sup>T<sub>E</sub>X style file.